

University of Dundee

Structural basis for RING-Cys-Relay E3 ligase activity and its role in axon integrity

Mabbitt, Peter D.; Loreto, Andrea; Déry, Marc-André; Fletcher, Adam J.; Stanley, Mathew; Pao, Kuan-Chuan

Published in:
Nature Chemical Biology

DOI:
[10.1038/s41589-020-0598-6](https://doi.org/10.1038/s41589-020-0598-6)

Publication date:
2020

Document Version
Peer reviewed version

[Link to publication in Discovery Research Portal](#)

Citation for published version (APA):

Mabbitt, P. D., Loreto, A., Déry, M-A., Fletcher, A. J., Stanley, M., Pao, K-C., Wood, N. T., Coleman, M. P., & Virdee, S. (2020). Structural basis for RING-Cys-Relay E3 ligase activity and its role in axon integrity. *Nature Chemical Biology*, 16(11), 1227-1236. <https://doi.org/10.1038/s41589-020-0598-6>

General rights

Copyright and moral rights for the publications made accessible in Discovery Research Portal are retained by the authors and/or other copyright owners and it is a condition of accessing publications that users recognise and abide by the legal requirements associated with these rights.

- Users may download and print one copy of any publication from Discovery Research Portal for the purpose of private study or research.
- You may not further distribute the material or use it for any profit-making activity or commercial gain.
- You may freely distribute the URL identifying the publication in the public portal.

Take down policy

If you believe that this document breaches copyright please contact us providing details, and we will remove access to the work immediately and investigate your claim.

Structural basis for RING-Cys-Relay E3 Ligase Activity and its Role in Axon Integrity

Peter D. Mabbitt¹, Andrea Loreto², Marc-André Déry¹, Adam J. Fletcher¹, Mathew Stanley³,
Kuan-Chuan Pao¹, Nicola T. Wood¹, Michael P. Coleman^{2,4} and Satpal Virdee^{1*}

¹MRC Protein Phosphorylation and Ubiquitylation Unit, University of Dundee, Scotland,
UK, DD1 5EH. ²John van Geest Centre for Brain Repair, University of Cambridge,
Cambridge, UK, CB2 0PY. ³Division of Gene Regulation and Expression, School of Life
Sciences, University of Dundee, Scotland, UK, DD1 5EH. ⁴The Babraham Institute,
Babraham Research Campus, Cambridge CB22 3AT, UK

* Corresponding author

Email: s.s.virdee@dundee.ac.uk

Tel: +44 (0)1382 388738

Fax: +44 (0)1382 388500

Abstract

MYCBP2 is a ubiquitin (Ub) E3 ligase (E3) that is essential for neurodevelopment and regulates axon maintenance. MYCBP2 transfers Ub to non-lysine substrates via a newly discovered RING-Cys-Relay (RCR) mechanism where Ub is relayed from an upstream cysteine to a downstream substrate esterification site. The molecular bases for E2-E3 Ub transfer and Ub relay are unknown. Whether these activities are linked to the neural phenotypes is also unclear. We describe the crystal structure of a covalently trapped E2-Ub:MYCBP2 transfer intermediate revealing key structural rearrangements upon E2-E3 Ub transfer and Ub relay. Our data suggest that transfer to the dynamic upstream cysteine, whilst mitigating lysine activity, requires a closed-like E2-Ub conjugate with tempered reactivity, and Ub relay is facilitated by a helix-coil transition. Furthermore, neurodevelopmental defects and delayed injury-induced degeneration in RCR-defective knock-in mice suggest its requirement, and that of substrate esterification activity, for normal neural development and programmed axon degeneration.

(150 words)

1 Main

2 Ubiquitination is a post-translational modification that regulates all aspects of
3 eukaryotic biology¹. Ubiquitin (Ub) transfer is initiated by an ATP-dependent Ub-activating
4 enzyme (E1). Ub is transferred from E1 to the catalytic cysteine of a ubiquitin-conjugating
5 enzyme (E2) via a chemical reaction known as transthiolation. The thioester-linked
6 intermediate (E2~Ub) is recruited by one of hundreds of ubiquitin E3 ligases (E3s), which
7 mediate discharge of Ub to specific substrates². Four distinct classes of E3 have been identified
8 but as our current understanding of E3 mechanism is based on a small subset of members, their
9 true diversity is likely to be unappreciated. The largest classification corresponds to RING/U-
10 Box E3s (referred to hereafter as RING E3s)³. RING E3s use an adaptor-like mechanism to
11 recruit the conformationally malleable E2~Ub conjugate⁴. RING E3s induce a folded back or
12 “closed” E2~Ub conformation which immobilizes the thioester, allosterically configures the
13 E2 active site for catalysis, and is a requisite for efficient aminolysis of a lysine acceptor⁵⁻⁹.
14 Maintenance of the closed conformation involves a network of interactions between E2 and
15 Ub. Activated RING E3 binding stabilizes these interactions thereby catalyzing substrate
16 ubiquitination⁷⁻⁹. In contrast, HECT and RBR E3 classes, that possess an essential catalytic
17 cysteine, undergo transthiolation with E2~Ub forming a covalent intermediate^{10,11}. Consistent
18 with the increased nucleophilicity of cysteine relative to lysine, HECT/RBR E3s engage
19 E2~Ub in a non-activating, “open” conformation^{9,12-16}. E3s that undergo transthiolation must
20 prevent inadvertent aminolysis activity and current experimental evidence supports the notion
21 that HECT/RBR E3s achieve this by enforcing the open conformation^{12,15,16}. These
22 observations imply that induction of the closed E2~Ub conformation is a specialised catalytic
23 feature reserved for adaptor-like E3 transfer to lysine acceptors and open conformations are
24 specialised, and sufficient, for transthiolation with cysteine.

25 MYCBP2 (also known as Phr1 (PAM-Highwire-Rpm-1)) is a conserved 0.5 MDa E3
26 with important roles in synaptogenesis and axon termination¹⁷⁻²². MYCBP2 has also been
27 shown to ubiquitinate Fbxw7 and ULK1 kinase thereby promoting chemotherapy resistance
28 and inhibiting neuronal autophagy, respectively^{23,24}. MYCBP2 was found to possess a novel
29 class of cysteine-dependent E3 machinery we termed RING-Cys-Relay (RCR)²⁵. Constitutive
30 *Phr1*^{-/-} mice (murine ortholog of MYCBP2) present with compromised axon development and
31 the phrenic nerve fails to fully innervate the diaphragm leading to perinatal respiratory failure²⁶.
32 However, conditional silencing of Phr1 in adult mice is tolerated and confers potent axon
33 protection *in vivo* and in *in vitro* primary neuron culture models of axon degeneration after
34 physical injury (Wallerian degeneration), or administration of the chemotherapeutic agent

vincristine²⁷. Thus, MYCBP2 is likely to have distinct roles in neural development and axon maintenance. Due to its latter role it has become a potential therapeutic target for a range of neurological conditions and neurodegenerative diseases²⁸.

The MYCBP2 RCR machinery utilises a RING domain that is presumed to bind E2^{25,29}. However, the RING domain is linked to a Tandem Cysteine (TC) domain containing two catalytic cysteine residues²⁵. The upstream cysteine undergoes transthiolation with E2~Ub and a subsequent step, termed Ub relay, shuttles Ub to the downstream cysteine by means of intramolecular transthiolation. The downstream site has esterification activity with selectivity for threonine²⁵. A crystal structure of the RCR machinery has revealed the general architecture of the TC domain and the basis for threonine-esterification activity²⁵. However, neither an E2~Ub:RCR transfer complex nor the upstream catalytic site (referred to as the mediator loop) have been structurally resolved. Thus, the molecular bases for E2~Ub recruitment, E2-E3 transthiolation and Ub relay are unknown. Furthermore, it remains unknown if loss of MYCBP2's unusual RING-linked RCR mechanism (i.e. E2-E3 transthiolation followed by Ub relay, and substrate esterification), is central to the neurodevelopmental and axon protective phenotypes.

Here we use a chemically engineered E2~Ub conjugate as a suicide substrate^{25,30}, which permits chemical stabilization of the dynamic mediator loop and the otherwise transient tetrahedral E2~Ub:RCR transfer intermediate. We solve the crystal structure of this transfer complex which reveals that MYCBP2 seemingly employs a distinct form of the closed E2~Ub conjugate associated with an attenuated state of thioester activation. Our data suggest this compensates for the dynamic nature of the upstream MYCBP2 catalytic cysteine whilst mitigating lysine activity. The structure also reveals novel RING-E2 recognition elements and insights into the unexpected incompatibility with a cysteine-reactive E2. We find the mediator loop region, disordered in the apo structure, adopts a short α -helix upon E2-E3 transthiolation. Surprisingly, mutational analysis of the mediator loop reveals that both E2-E3 transthiolation and Ub relay are highly robust processes. However, whilst helix disrupting proline mutations in general do not affect E2-E3 transthiolation, they impair Ub relay. This suggests that transient helix formation is requisite for Ub relay, which we propose is mediated by an entropically-driven helix-coil transition. To assess whether loss of RCR E3 activity is linked to the neural phenotypes we generate upstream cysteine mutant (*Phr1*^{C4629A/C4629A}) mice where E2-E3 transthiolation, subsequent relay, and substrate esterification activity are abolished. Remarkably, we find that the neurodevelopmental and axon protective phenotypes presented

1 in null animals are recapitulated in *Phr1*^{C4629A/C4629A} mouse neurons indicating that loss of
2 MYCBP2 RCR activity is central to these phenotypes.

3 4 5 **Results**

6 7 **Structure determination of the E2-E3 transfer intermediate**

8
9 Although chemical engineering approaches have been instrumental for the stabilization
10 and structural resolution of the conformationally dynamic transfer intermediates associated
11 with Ub conjugation³¹⁻³³, structural resolution of a tetrahedral, enzymatic ubiquitin-acyl donor
12 intermediate has not been reported for any E3 classification. A previously described activity-
13 based probe (ABP) based on a chemically engineered E2~Ub conjugate, functions as a suicide
14 substrate for E3 transthiolation^{25,30} (Fig. 1a, b). We used this ABP to covalently modify the
15 RCR, enabling stabilization of the dynamic mediator loop and the transient E2-E3 Ub transfer
16 complex (Fig. 1b). Importantly, ABP E3 catalytic cysteine labelling forms a tetrahedral
17 *bisthioether* that locally recapitulates the geometry of the anticipated tetrahedral Ub
18 transthiolation intermediate (Fig. 1b). Diffracting crystals of the engineered covalent
19 E2~Ub:RCR complex were obtained and a structural model was refined to 2.58 Å (Fig. 1c–e
20 and Extended Data Figs. 1–3).

21 22 **The RCR E3 engages a closed-like E2~Ub conformation**

23
24 Our structure accurately recapitulates a transition state intermediate for Ub transfer
25 from E2 to the upstream Cys4520 residue within the E3 mediator loop. The mediator loop is
26 now found to be structured and forms a short α -helix (Fig. 1d, e). Mediator loop residues do
27 not appear to catalytically participate in the transfer process. Rather, transfer to the upstream
28 cysteine residue is facilitated by the RCR binding E2~Ub in a closed conformation, which is
29 entirely distinct from reported catalytic-cysteine dependent E3s^{12,13,15,16}. However, a $\sim 30^\circ$
30 rotation of the Ub molecule, centering on Ub Ile44, alters the closed E2~Ub conformation (Fig.
31 2a). Rotation maintains the highly conserved Ub Ile44 interaction with E2 crossover helix
32 residue Leu104^{5,6}, which is dispensable for HECT/RBR activity⁹. Other interactions with the
33 globular Ub fold, previously identified as essential for canonical ‘closed’ E2~Ub activation to

lysine acceptors, are also largely maintained in the RCR:E2~Ub complex (Fig. 2b, 2c, Extended Data Fig. 4-5). There are two notable exceptions. Firstly, an interaction between Ub Ile36 and the RING domain is lost (Extended Data Fig. 4b). Typically, alanine mutation at this site abolishes canonical activity^{7,8}. Consistent with this interaction being dispensable for activity, a Ub I36A mutant only decreases RCR activity by ~50 % (Fig. 2c). Partial dependence might be reconciled by an intramolecular Ile36 side chain interaction with Leu71 in the Ub tail (Extended Data Fig. 5a). Secondly, the RCR complex lacks the so-called “linchpin” interactions between a conserved arginine/lysine residue within the RING domain⁹. Prototypical RING/E2~Ub complexes have this residue forming bivalent hydrogen-bonds between E2 Gln92, Ub Gln40 and Ub Arg72 (Extended Data Fig. 4b)⁷⁻⁹. These interactions contribute to anchoring the carboxy terminus of Ub into the E2 active site groove and are considered important for optimum thioester immobilization and E2 active site configuration as their disruption leads to undetectable/negligible activity⁷⁻⁹. In the RCR complex the Ub rotation shifts Ub Arg72 ~12 Å away from linchpin Lys4441, abolishing its interaction with the E2 Gln92 backbone and Ub Gln40 (Extended Data Fig. 4b). Consistent with a relaxed role, activity of an RCR Lys4441Ala mutant was reduced only by 40 % and a Ub Gln40Ala mutant was unaffected (Fig. 2c)⁷. A presumed consequence of the lack of these two key canonical interactions would be an intermediate state of thioester activation relative to previously reported RING exemplars.

Ubiquitin transfer to the RCR requires E2~Ub activation

As our structure geometrically recapitulates a covalently trapped E2~Ub acyl donor intermediate, the orientation of active site residues during catalysis can be inferred (Fig. 2d, Extended Data Fig. 4b). We find that as previously proposed for closed E2~Ub activation, catalysis hinges on E2 Asn77. Canonical closed E2~Ub activation leads to an active site configuration that brings the essential Asn77 residue into proximity of the thioester carbonyl oxygen atom in E2~Ub^{7,11,34,35}. Here, Asn77 might catalytically activate E2~Ub to lysine nucleophilic attack by stabilizing the transient negative charge that forms on the thioester-derived oxygen atom in the tetrahedral transfer intermediate. Alternately, Asn77 may act indirectly by hydrogen bonding to the backbone of Asn114 and stabilize the E2 active-site loop containing Asp117 (Fig. 2d)^{36,37}. A role in thioester immobilization has also been proposed³⁸. As Asn77 is dispensable for HECT/RBR activity it is thought these requirements are a hallmark of a closed E2~Ub activation mechanism for lysine acceptors^{11,13}.

Consistent with our complex, the dependence on Asn77 for RCR activity underscores the unexpected requirement for closed-like E2~Ub activation for transthiolation with MYCBP2 (Fig. 2c). In our transthiolation complex, Asn77 is geometrically compatible with stabilizing the transient negative charge on the thioester-derived oxygen atom, yet we also observe the interaction between Asn77 and the backbone of Asn114 (Fig. 2d, Extended Data Fig. 4-5). Hence, to elucidate if Asn77 has a particular role in E2-MYCBP2 Ub transfer we determined observed rate constants for Asn77Ser, Asn114Ala, Asp117Ala, and a Asn114Ala Asp117Ala double mutant (Extended Data Fig. 4e-i). In addition to kinetically quantifying the mutants in single turnover C4520K isopeptide assays, we also assessed native cysteine transthiolation activity, thereby allowing potential acceptor-specific roles to be uncovered (Extended Data Fig. 4i, 5e-i)). Strikingly, the observed rates for native transthiolation for Asp117Ala and the Asn114Ala Asp117Ala double mutant were indistinguishable from WT E2, indicative of the described structural role of Asn77 being dispensable. However, the Asn77Ser mutant had no detectable activity (Extended Data Fig. 4i, 5f). This suggests that Asn77's role in MYCBP2 transthiolation is tetrahedral intermediate stabilization and/or thioester immobilization; both of which are consistent with our structure (Fig. 2d). In contrast, in the isopeptide assay lysine aminolysis was undetectable upon mutation of Asp117, demonstrating that its role is likely to be specific for lysine acceptors where it has been shown to position the lysine ϵ -amino group and/or suppress its pK_a ^{35,37,38}. Consistent with interactions towards the Asn114 backbone being key^{7,36}, Asn114Ala rates were comparable to WT. However, our data cannot exclude the possibility that alternative structural roles mediated by Asn77 may facilitate lysine aminolysis³⁶.

Independent of Asn77, E2 Asp87 augments the canonical linchpin interaction by further anchoring the Ub C-terminus by interaction with Ub Arg74. This interaction was thought to only be required for lysine acceptors^{7,8,11}. We find this interaction also remains critical further underscoring the unusual closed-like requirement for MYCBP2 transthiolation with E2 (Fig. 2c, d, Extended Data Fig. 4d).

E2~Ub activation compensates for mediator loop entropy

An explanation for why transfer to cysteine in the context of the RCR requires E2~Ub activation whereas HECT/RBR E3s do not is that whilst the dynamic nature of the upstream cysteine will not affect intrinsic sulfhydryl reactivity, it might compromise its ability to serve

1 as an effective nucleophile³⁹. The lack of the linchpin and Ub Ile36 interactions would be
2 expected to compromise the stability of the closed conformation that catalytically configures
3 the active site. In turn, this would attenuate thioester reactivity. However, as MYCBP2 is a
4 non-lysine E3 ligase²⁵, aminolysis activity must be mitigated. Thus, employment of a tempered
5 form of the E2~Ub conjugate could satisfy the requirements for elevated reactivity to mediate
6 transthiolation with the mobile upstream cysteine whilst remaining below the threshold for
7 lysine aminolysis activity. To test if the rotated form of the E2~Ub intermediate engaged by
8 the RCR had attenuated reactivity we turned to a version of the RCR where Cys4520 is mutated
9 to alanine. This abolishes competition with native E2-E3 transthiolation allowing assessment
10 of enhanced rate of Ub discharge to free lysine¹¹. We found that RCR Cys4520Ala did not
11 enhance lysine discharge activity, supportive of the E2~Ub conformation engaged by
12 MYCBP2 having attenuated reactivity relative to model, dimeric RING E3 systems (Extended
13 Data Fig. 5j)⁷⁻⁹. Although the crystallographic Ub rotation could account for the attenuated
14 E2~Ub reactivity we observe, we cannot formally exclude the former is imparted by crystal
15 packing and activity attenuation is achieved by an alternative mechanism (Extended Data Fig.
16 6).

MYCBP2 RING–E2 interface

It was previously assumed that the RCR RING domain binds E2 and the structure reveals that a canonical interface is largely adopted albeit with distinct molecular contacts (Fig. 3a, 3c, Extended Data Fig. 7). Consistent with a closed-like E2~Ub conformation, there is no RING insertion to prevent its formation^{15,16} (Extended Data Fig. 7h). In fact, the contrary appears to be the case as the helix-turn-helix motif renders the RCR incompatible with an open conformation (Extended Data Fig. 8a) Hence, a role for the helix-turn-helix motif might be to prevent engagement of an open E2~Ub conjugate, which based on our observations would be catalytically unproductive.

Interactions between the MYCBP2 RING domain and E2 shared with canonical RING-E2 interactions include the E2 loop 2 residue Pro95 engaging the core of the RING (Ile4392, Phe4394, Val4420, and Pro4438) (Fig. 3a, Extended Data Fig. 9) and alanine mutation of Ile4392 or F4394 reduces RCR isopeptide formation by ~30 % (Fig. 2c). A difference associated with the loop 1 interaction is that between E2 Phe62 and the RCR RING (Fig. 3a). Typically the Phe side chain docks into a shallow hydrophobic pocket within the RING domain and Phe mutation impairs or even abolishes canonical RING activity^{7,40}. In the case of the RCR RING, the Phe62 pocket is deeper and highly basic and complementarity toward Phe62 is now achieved via a cation-pi interaction with RING Arg4419 (Fig. 3a).

A striking feature of the RCR RING is its pronounced loop extension²⁵. The complexed structure reveals that this serves as an extended docking site for E2 where it complements an E2 region not previously implicated with RING binding (Fig. 3b). In this context, E2 Arg90 H-bonds to Leu4426 within the RING extension. To probe this interaction, we mutated E2 Arg90 to Ala and made a charge-swapped Arg90Glu mutant. Its importance is supported as activity drops by 40 % and 70 %, respectively (Fig. 2c). However, E2-RING recognition is cumulative as even a double Ile4392Ala Leu4426Ala mutant that disrupts both the RING extension and the canonical interface retained 20 % activity (Fig. 3c).

An anomalous characteristic of the RCR is that despite being an E3 that undergoes transthiolation, it is not functional with the E2 UBE2L3²⁵, which was understood to support E3 transthiolation activity with most, if not all, catalytic cysteine-dependent E3s¹¹. Our structural insights reveal that incompatibility with UBE2L3 can be primarily ascribed to the presence of Lys96 (homologous to Ser94 in UBE2D3) which would clash with the MYCBP2 RING domain (Fig. 3d). However, we could not impart UBE2L3 compatibility by mutation of the

offending Lys96 to serine suggesting that inactivity might be multifactorial (Extended Data Fig. 8b).

Ubiquitin relay is mediated by a helix-coil transition

Strikingly, our structure reveals that during E2-E3 Ub transfer the disordered mediator loop transiently adopts an ordered helical conformation (Fig. 4a). This implies that once MYCBP2 Cys4520 has been thioesterified with Ub, subsequent relay to the downstream Cys4572 residue would require a distance of at least ~21 Å to be traversed to facilitate intramolecular transthiolation (Fig. 4a). Analogous intramolecular peptide acyl transfer reactions have been observed in simple organisms⁴¹, where the tertiary structure of the enzyme brings acyl donor and nucleophilic acceptor in close proximity⁴². However, in the case of RCR Ub relay, substantial remodelling of the mediator “loop’s” pre-helical state would be required²⁵. We tested the side chain properties of selected mediator loop residues for a potential role in Ub relay using an alanine scan. To deconvolute defects in E2-E3 transthiolation from Ub relay, which are concerted, we initially assessed Cys4520~Ub thioester formation independently (Fig. 4b), prior to assessment of Ub relay to a dead-end product (Fig. 4c). With the exception of the C4520A mutant, which abolishes thioester formation as expected, all alanine mutants retain WT levels of E2-E3 transthiolation activity (Fig. 4d). Strikingly, Ub relay was also found to be extremely robust and unperturbed by any of the side chain mutations (Fig. 4e). Ablation of E2-E3 transthiolation and Ub relay required an amino acid deletion (Δ A4518) upstream of Cys4520 (Fig. 4a, Extended Data Fig. 8c-d).

The permissive nature of the mediator loop led us to consider backbone perturbation using a proline scan where mutation would render helix formation less thermodynamically favourable⁴³. Whereas this largely does not perturb E2-E3 transthiolation (Fig. 4f), all proline substitutions impair Ub relay (Fig. 4g). The most severe substitutions tend to be at sites immediately proximal of Cys4520 where Ala4518Pro and Asp4521Pro reduce relay by 80 % and 70 %, respectively. These observations suggest that whilst helix formation is not necessary for E2-E3 transthiolation, it is required for efficient Ub relay. As the mediator loop was found to be fully disordered in the apo structure²⁵, and has elevated B-factors in our transfer complex (Extended data Fig. 2d, e), we propose Ub relay is facilitated by the mediator loop undergoing an entropically-driven helix-coil transition. Helix-coil transitions have been studied extensively in model peptides^{44,45}, but to our knowledge, have not been directly implicated with catalysis.

RCR is central to neurodevelopment and axon protection

Loss of MYCBP2 E3 ligase activity is likely to be central to the axon protective phenotype as RING mutants in *Drosophila* cells stabilize the axon survival factor NMNAT2²⁹. However, it is unclear whether loss of E2-E3 transthiolation, intramolecular Ub relay, and substrate esterification are linked to the neural phenotypes. We generated homozygous knock-in mice that express an orthologous upstream cysteine to alanine mutant rendering all aspects of RCR activity defective (*Phr1*^{C4629A/C4629A}). Expression levels of *Phr1* were found to be consistent across genotypes (Extended Data Fig. 10a), Activity-based proteomics and gel shift analysis of mouse embryonic fibroblasts (MEFs) also confirmed RCR E3 activity was abolished in homozygous samples (Fig. 5a, Extended Data Fig. 10b, c). Furthermore, expression levels of the *Phr1* substrate NMNAT2 when transiently expressed in MEFs were elevated in homozygous samples (Extended Data Fig. 10d). To assess whether loss of RCR activity specifically is likely to recapitulate perinatal lethality observed with null mice, we imaged innervation of the diaphragm by the phrenic nerve in embryonic day 18 (E18.5) mice (Fig. 5b)^{19,21,22,26}. Consistent with previous studies with null mice we found defective innervation of the diaphragm in *Phr1*^{C4629A/C4629A} relative to *Phr1*^{C4629A/+}, as shown by the marked reduction of secondary branches of the phrenic nerve (Fig. 5b, Extended Data Fig. 10e). Stunting of neurite outgrowth was also observed in primary superior cervical ganglion (SCG) neurons from E18.5 *Phr1*^{C4629A/C4629A} mice relative to wild-type and heterozygous littermates (Fig. 5c, d).

Next, we tested the stunted neurites for axon protection in transection assays. Remarkably, despite starting from a higher base, absolute degeneration index measurements are significantly lower at 8 hours post injury indicating neurite protection ($P \leq 0.0001$) (Fig. 5e, f). To normalise for reduced neurite growth and health in *Phr1*^{C4629A/C4629A} mice relative to *Phr1*^{+/+} and *Phr1*^{C4629A/+} (resulting in a higher absolute degeneration index at time 0 h), we also measured change in degeneration index⁴⁶ (Fig. 5f). In these cultures it is impossible to separate the effects of the developmental phenotype from axon protection, but the stunted growth of the *Phr1*^{C4629A/C4629A} appears more likely to partially mask the protective effect than to contribute to it. These results indicate that loss of the novel RCR mechanism, followed by substrate esterification, is responsible for the neurodevelopmental defects and axon protection in adult mice (Fig. 6). Thus, inhibition of the RCR mechanism in adult animals could be a valuable

strategy for the treatment of neurodegenerative diseases and neurologic disorders linked to axonal degeneration.

Discussion

The discovery that MYCBP2 RCR uses catalytic features hitherto considered the reserve of canonical RING E3s demonstrates the unappreciated diversity of E3 ligases. Our study demonstrates that RING domains can stabilize closed E2~Ub conformations to facilitate Ub transfer to not only lysine, but also cysteine. The extent of E2~Ub activation can be modulated by the E3 depending on the context of the acceptor site. We anticipate that this mechanism is adopted more widely by the hundreds of RING E3s for substrate ubiquitination. Highly templated and sterically unhindered sites may also be ubiquitinated by a similarly intermediate state of RING-mediated E2~Ub activation, whereas robust stabilization of the closed, activated state might be reserved for more dynamically and sterically challenging sites. Indeed, it has been shown that RING E3s can demonstrate attenuated activity as a means of tuning substrate specificity⁴⁷. The engineered suicide substrate approach enabled structural elucidation of a highly transient rate-limiting helical intermediate and granted insights into the Ub relay process. Our proposal that Ub relay is mediated by a helix-coil transition provides a framework for how intrinsic disorder might directly facilitate ubiquitin transfer and enzyme catalysis more generally.

We establish that the mechanistically non-homologous Ub relay and non-lysine esterification activities demonstrated by MYCBP2 are likely to be central to the axon protective phenotypes. Our latter inference is based on the observation that MYCBP2 has no lysine activity and will in fact inhibit intrinsic E2 lysine activity through non-productive E2-E3 transthiolation²⁵. The most likely target of MYCBP2 non-lysine E3 activity is NMNAT2^{27,29}, either through direct or indirect ubiquitination and destabilization. This presents an exciting therapeutic opportunity for pharmacologically inhibiting Wallerian-like axon degeneration which has been implicated with a number of neurological conditions such as neuropathies and neurodegenerative diseases²⁸. Indeed, one protein downstream of MYCBP2 is SARM1, which is another positive regulator of the Wallerian process⁴⁸. The discovery of SARM1 having enzymatic activity has led to it becoming an attractive therapeutic target^{49,50}. The structural and biochemical insights obtained herein pertaining to MYCBP2 could similarly inform and accelerate the development of therapeutics.

Acknowledgments

We thank Jin-Feng Zhao, Gail Gilmour, Mehreen Mohammad, Joby Varghese, and Axel Knebel of the MRC Protein Phosphorylation and Ubiquitylation Unit. We thank the European Synchrotron Radiation Facility (ESRF). This work was funded by UK Medical Research Council (MC_UU_12016/8) and Biotechnology and Biological Sciences Research Council (BB/P003982/1). A.L. was funded by a Sir Henry Wellcome Postdoctoral Fellowship from the Wellcome Trust (210904/Z/18/Z). We also acknowledge pharmaceutical companies supporting the Division of Signal Transduction Therapy (Boehringer-Ingelheim, GlaxoSmithKline and Merck KGaA).

Authors contributions

S.V conceived research. P.D.M. designed and carried out experiments. M.C. and A.L. designed diaphragm imaging and neuron explant experiments that were carried out by A.L. M-A.D. coordinated animal breeding and obtained and characterised MEF samples by immunoblot and ABP gel-shift analysis. A.J.F. Prepared MBP-tagged probe and carried out activity-based proteomics and data processing. M.S., K-C.P. synthesized reagents. N.T.W. designed and made cDNA constructs. S.V. and P.D.M. wrote the manuscript with input from other authors.

Competing interest

S.V., K.-C.P. and M.S. are authors on patents relating to work presented in this article.

References

- 1 Komander, D. & Rape, M. The ubiquitin code. *Annu Rev Biochem* **81**, 203-229, doi:10.1146/annurev-biochem-060310-170328 (2012).
- 2 Oh, E., Akopian, D. & Rape, M. Principles of Ubiquitin-Dependent Signaling. *Annu Rev Cell Dev Biol* **34**, 137-162, doi:10.1146/annurev-cellbio-100617-062802 (2018).
- 3 Deshaies, R. J. & Joazeiro, C. A. RING domain E3 ubiquitin ligases. *Annu Rev Biochem* **78**, 399-434, doi:10.1146/annurev.biochem.78.101807.093809 (2009).
- 4 Pruneda, J. N., Stoll, K. E., Bolton, L. J., Brzovic, P. S. & Klevit, R. E. Ubiquitin in motion: structural studies of the ubiquitin conjugating enzyme~ubiquitin conjugate. *Biochemistry* **50**, 1624-1633, doi:10.1021/bi101913m (2011).
- 5 Saha, A., Lewis, S., Kleiger, G., Kuhlman, B. & Deshaies, R. J. Essential role for ubiquitin-ubiquitin-conjugating enzyme interaction in ubiquitin discharge from Cdc34 to substrate. *Mol Cell* **42**, 75-83, doi:10.1016/j.molcel.2011.03.016 (2011).
- 6 Wickliffe, K. E., Lorenz, S., Wemmer, D. E., Kuriyan, J. & Rape, M. The mechanism of linkage-specific ubiquitin chain elongation by a single-subunit E2. *Cell* **144**, 769-781, doi:10.1016/j.cell.2011.01.035 (2011).
- 7 Plechanovova, A., Jaffray, E. G., Tatham, M. H., Naismith, J. H. & Hay, R. T. Structure of a RING E3 ligase and ubiquitin-loaded E2 primed for catalysis. *Nature* **489**, 115-120, doi:10.1038/nature11376 (2012).
- 8 Dou, H., Buetow, L., Sibbet, G. J., Cameron, K. & Huang, D. T. BIRC7-E2 ubiquitin conjugate structure reveals the mechanism of ubiquitin transfer by a RING dimer. *Nat Struct Mol Biol* **19**, 876-883, doi:10.1038/nsmb.2379 (2012).
- 9 Pruneda, J. N. *et al.* Structure of an E3:E2~Ub Complex Reveals an Allosteric Mechanism Shared among RING/U-box Ligases. *Mol Cell* **47**, 933-942, doi:10.1016/j.molcel.2012.07.001 (2012).
- 10 Scheffner, M., Nuber, U. & Huibregtse, J. M. Protein ubiquitination involving an E1-E2-E3 enzyme ubiquitin thioester cascade. *Nature* **373**, 81-83, doi:10.1038/373081a0 (1995).
- 11 Wenzel, D. M., Lissounov, A., Brzovic, P. S. & Klevit, R. E. UBC7 reactivity profile reveals parkin and HHARI to be RING/HECT hybrids. *Nature* **474**, 105-108, doi:10.1038/nature09966 (2011).
- 12 Kamadurai, H. B. *et al.* Insights into ubiquitin transfer cascades from a structure of a UbcH5B~ubiquitin-HECT(NEDD4L) complex. *Mol Cell* **36**, 1095-1102, doi:10.1016/j.molcel.2009.11.010 (2009).
- 13 Lechtenberg, B. C. *et al.* Structure of a HOIP/E2~ubiquitin complex reveals RBR E3 ligase mechanism and regulation. *Nature* **529**, 546-550, doi:10.1038/nature16511 (2016).
- 14 Dove, K. K., Stieglitz, B., Duncan, E. D., Rittinger, K. & Klevit, R. E. Molecular insights into RBR E3 ligase ubiquitin transfer mechanisms. *Embo Rep* **17**, 1221-1235, doi:10.15252/embr.201642641 (2016).
- 15 Dove, K. K. *et al.* Structural Studies of HHARI/UbcH7~Ub Reveal Unique E2~Ub Conformational Restriction by RBR RING1. *Structure* **25**, 890-900 e895, doi:10.1016/j.str.2017.04.013 (2017).
- 16 Yuan, L., Lv, Z., Atkison, J. H. & Olsen, S. K. Structural insights into the mechanism and E2 specificity of the RBR E3 ubiquitin ligase HHARI. *Nat Commun* **8**, 211, doi:10.1038/s41467-017-00272-6 (2017).
- 17 Wan, H. I. *et al.* Highwire regulates synaptic growth in Drosophila. *Neuron* **26**, 313-329, doi:10.1016/s0896-6273(00)81166-6 (2000).

- 1 18 Zhen, M., Huang, X., Bamber, B. & Jin, Y. Regulation of presynaptic terminal
2 organization by *C. elegans* RPM-1, a putative guanine nucleotide exchanger with a
3 RING-H2 finger domain. *Neuron* **26**, 331-343, doi:10.1016/s0896-6273(00)81167-8
4 (2000).
- 5 19 Schaefer, A. M., Hadwiger, G. D. & Nonet, M. L. rpm-1, a conserved neuronal gene
6 that regulates targeting and synaptogenesis in *C. elegans*. *Neuron* **26**, 345-356,
7 doi:10.1016/s0896-6273(00)81168-x (2000).
- 8 20 D'Souza, J. *et al.* Formation of the retinotectal projection requires Esrom, an ortholog
9 of PAM (protein associated with Myc). *Development* **132**, 247-256,
10 doi:10.1242/dev.01578 (2005).
- 11 21 Bloom, A. J., Miller, B. R., Sanes, J. R. & DiAntonio, A. The requirement for Phr1 in
12 CNS axon tract formation reveals the corticostriatal boundary as a choice point for
13 cortical axons. *Genes Dev* **21**, 2593-2606, doi:10.1101/gad.1592107 (2007).
- 14 22 Lewcock, J. W., Genoud, N., Lettieri, K. & Pfaff, S. L. The ubiquitin ligase Phr1
15 regulates axon outgrowth through modulation of microtubule dynamics. *Neuron* **56**,
16 604-620, doi:10.1016/j.neuron.2007.09.009 (2007).
- 17 23 Richter, K. T., Kschonsak, Y. T., Vodicska, B. & Hoffmann, I. FBXO45-MYCBP2
18 regulates mitotic cell fate by targeting FBXW7 for degradation. *Cell Death Differ*,
19 doi:10.1038/s41418-019-0385-7 (2019).
- 20 24 Crawley, O. *et al.* Autophagy is inhibited by ubiquitin ligase activity in the nervous
21 system. *Nat Commun* **10**, 5017, doi:10.1038/s41467-019-12804-3 (2019).
- 22 25 Pao, K. C. *et al.* Activity-based E3 ligase profiling uncovers an E3 ligase with
23 esterification activity. *Nature* **556**, 381-385, doi:10.1038/s41586-018-0026-1 (2018).
- 24 26 Burgess, R. W. *et al.* Evidence for a conserved function in synapse formation reveals
25 Phr1 as a candidate gene for respiratory failure in newborn mice. *Mol Cell Biol* **24**,
26 1096-1105, doi:10.1128/mcb.24.3.1096-1105.2004 (2004).
- 27 27 Babetto, E., Beirowski, B., Russler, E. V., Milbrandt, J. & DiAntonio, A. The Phr1
28 Ubiquitin Ligase Promotes Injury-Induced Axon Self-Destruction. *Cell Rep* **3**, 1422-
29 1429, doi:10.1016/j.celrep.2013.04.013 (2013).
- 30 28 Coleman, M. P. & Hoke, A. Programmed axon degeneration: from mouse to
31 mechanism to medicine. *Nat Rev Neurosci* **21**, 183-196, doi:10.1038/s41583-020-
32 0269-3 (2020).
- 33 29 Xiong, X. *et al.* The Highwire ubiquitin ligase promotes axonal degeneration by tuning
34 levels of Nmnat protein. *PLoS Biol* **10**, e1001440, doi:10.1371/journal.pbio.1001440
35 (2012).
- 36 30 Pao, K. C. *et al.* Probes of ubiquitin E3 ligases enable systematic dissection of parkin
37 activation. *Nat Chem Biol* **12**, 324-331, doi:10.1038/nchembio.2045 (2016).
- 38 31 Olsen, S. K., Capili, A. D., Lu, X., Tan, D. S. & Lima, C. D. Active site remodelling
39 accompanies thioester bond formation in the SUMO E1. *Nature* **463**, 906-912,
40 doi:10.1038/nature08765 (2010).
- 41 32 Kamadurai, H. B. *et al.* Mechanism of ubiquitin ligation and lysine prioritization by a
42 HECT E3. *Elife* **2**, e00828, doi:10.7554/eLife.00828 (2013).
- 43 33 Streich, F. C., Jr. & Lima, C. D. Capturing a substrate in an activated RING E3/E2-
44 SUMO complex. *Nature* **536**, 304-308, doi:10.1038/nature19071 (2016).
- 45 34 Wu, P. Y. *et al.* A conserved catalytic residue in the ubiquitin-conjugating enzyme
46 family. *EMBO J* **22**, 5241-5250, doi:10.1093/emboj/cdg501 (2003).
- 47 35 Yunus, A. A. & Lima, C. D. Lysine activation and functional analysis of E2-mediated
48 conjugation in the SUMO pathway. *Nature Structural & Molecular Biology* **13**, 491-
49 499, doi:10.1038/nsmb1104 (2006).

- 36 Berndsen, C. E., Wiener, R., Yu, I. W., Ringel, A. E. & Wolberger, C. A conserved asparagine has a structural role in ubiquitin-conjugating enzymes. *Nat Chem Biol* **9**, 154-156, doi:10.1038/nchembio.1159 (2013).
- 37 Wilson, R. H., Zamfir, S. & Sumner, I. Molecular dynamics simulations reveal a new role for a conserved active site asparagine in a ubiquitin-conjugating enzyme. *J Mol Graph Model* **76**, 403-411, doi:10.1016/j.jmglm.2017.07.006 (2017).
- 38 Jones, W. M., Davis, A. G., Wilson, R. H., Elliott, K. L. & Sumner, I. A conserved asparagine in a ubiquitin-conjugating enzyme positions the substrate for nucleophilic attack. *J Comput Chem* **40**, 1969-1977, doi:10.1002/jcc.25852 (2019).
- 39 Bruice, T. C. & Pandit, U. K. Intramolecular Models Depicting the Kinetic Importance of "Fit" in Enzymatic Catalysis. *Proc Natl Acad Sci U S A* **46**, 402-404, doi:10.1073/pnas.46.4.402 (1960).
- 40 Zheng, N., Wang, P., Jeffrey, P. D. & Pavletich, N. P. Structure of a c-Cbl-UbcH7 complex: RING domain function in ubiquitin-protein ligases. *Cell* **102**, 533-539, doi:10.1016/s0092-8674(00)00057-x (2000).
- 41 Mills, K. V., Johnson, M. A. & Perler, F. B. Protein splicing: how inteins escape from precursor proteins. *J Biol Chem* **289**, 14498-14505, doi:10.1074/jbc.R113.540310 (2014).
- 42 Klabunde, T., Sharma, S., Telenti, A., Jacobs, W. R., Jr. & Sacchettini, J. C. Crystal structure of GyrA intein from *Mycobacterium xenopi* reveals structural basis of protein splicing. *Nat Struct Biol* **5**, 31-36 (1998).
- 43 Oneil, K. T. & Degrado, W. F. A Thermodynamic Scale for the Helix-Forming Tendencies of the Commonly Occurring Amino-Acids. *Science* **250**, 646-651, doi:DOI 10.1126/science.2237415 (1990).
- 44 Schellman, J. A. The Factors Affecting the Stability of Hydrogen-Bonded Polypeptide Structures in Solution. *J Phys Chem-Us* **62**, 1485-1494 (1959).
- 45 Zimm, B. H. & Bragg, J. K. Theory of the Phase Transition between Helix and Random Coil in Polypeptide Chains. *J Chem Phys* **31**, 526-535, doi:Doi 10.1063/1.1730390 (1959).
- 46 Gilley, J., Mayer, P. R., Yu, G. & Coleman, M. P. Low levels of NMNAT2 compromise axon development and survival. *Hum Mol Genet* **28**, 448-458, doi:10.1093/hmg/ddy356 (2019).
- 47 Stewart, M. D. *et al.* Tuning BRCA1 and BARD1 activity to investigate RING ubiquitin ligase mechanisms. *Protein Sci* **26**, 475-483, doi:10.1002/pro.3091 (2017).
- 48 Osterloh, J. M. *et al.* dSarm/Sarm1 is required for activation of an injury-induced axon death pathway. *Science* **337**, 481-484, doi:10.1126/science.1223899 (2012).
- 49 Essuman, K. *et al.* The SARM1 Toll/Interleukin-1 Receptor Domain Possesses Intrinsic NAD(+) Cleavage Activity that Promotes Pathological Axonal Degeneration. *Neuron* **93**, 1334-1343 e1335, doi:10.1016/j.neuron.2017.02.022 (2017).
- 50 Loring, H. S. & Thompson, P. R. Emergence of SARM1 as a Potential Therapeutic Target for Wallerian-type Diseases. *Cell Chem Biol* **27**, 1-13, doi:10.1016/j.chembiol.2019.11.002 (2020).
- 51 Kabsch, W. Xds. *Acta Crystallogr D Biol Crystallogr* **66**, 125-132, doi:10.1107/S0907444909047337 (2010).
- 52 Evans, P. R. & Murshudov, G. N. How good are my data and what is the resolution? *Acta Crystallogr D* **69**, 1204-1214, doi:10.1107/S0907444913000061 (2013).
- 53 McCoy, A. J. *et al.* Phaser crystallographic software. *J Appl Crystallogr* **40**, 658-674, doi:10.1107/S0021889807021206 (2007).

- 1 54 Emsley, P., Lohkamp, B., Scott, W. G. & Cowtan, K. Features and development of
2 Coot. *Acta Crystallogr D Biol Crystallogr* **66**, 486-501,
3 doi:10.1107/S0907444910007493 (2010).
- 4 55 Murshudov, G. N. *et al.* REFMAC5 for the refinement of macromolecular crystal
5 structures. *Acta Crystallogr D Biol Crystallogr* **67**, 355-367,
6 doi:10.1107/S0907444911001314 (2011).
- 7 56 Moriarty, N. W., Grosse-Kunstleve, R. W. & Adams, P. D. electronic Ligand Builder
8 and Optimization Workbench (eLBOW): a tool for ligand coordinate and restraint
9 generation. *Acta Crystallogr D Biol Crystallogr* **65**, 1074-1080,
10 doi:10.1107/S0907444909029436 (2009).
- 11 57 Afonine, P. V. *et al.* FEM: feature-enhanced map. *Acta Crystallogr D Biol Crystallogr*
12 **71**, 646-666, doi:10.1107/S1399004714028132 (2015).
- 13 58 Brownell, J. E. *et al.* Substrate-assisted inhibition of ubiquitin-like protein-activating
14 enzymes: the NEDD8 E1 inhibitor MLN4924 forms a NEDD8-AMP mimetic in situ.
15 *Mol Cell* **37**, 102-111, doi:10.1016/j.molcel.2009.12.024 (2010).
- 16 59 Stanley, M. *et al.* Orthogonal thiol functionalization at a single atomic center for
17 profiling transthiolation activity of E1 activating enzymes. *ACS Chem Biol* **10**, 1542-
18 1554, doi:10.1021/acschembio.5b00118 (2015).
- 19 60 Sasaki, Y., Vohra, B. P., Lund, F. E. & Milbrandt, J. Nicotinamide mononucleotide
20 adenylyl transferase-mediated axonal protection requires enzymatic activity but not
21 increased levels of neuronal nicotinamide adenine dinucleotide. *J Neurosci* **29**, 5525-
22 5535, doi:10.1523/JNEUROSCI.5469-08.2009 (2009).

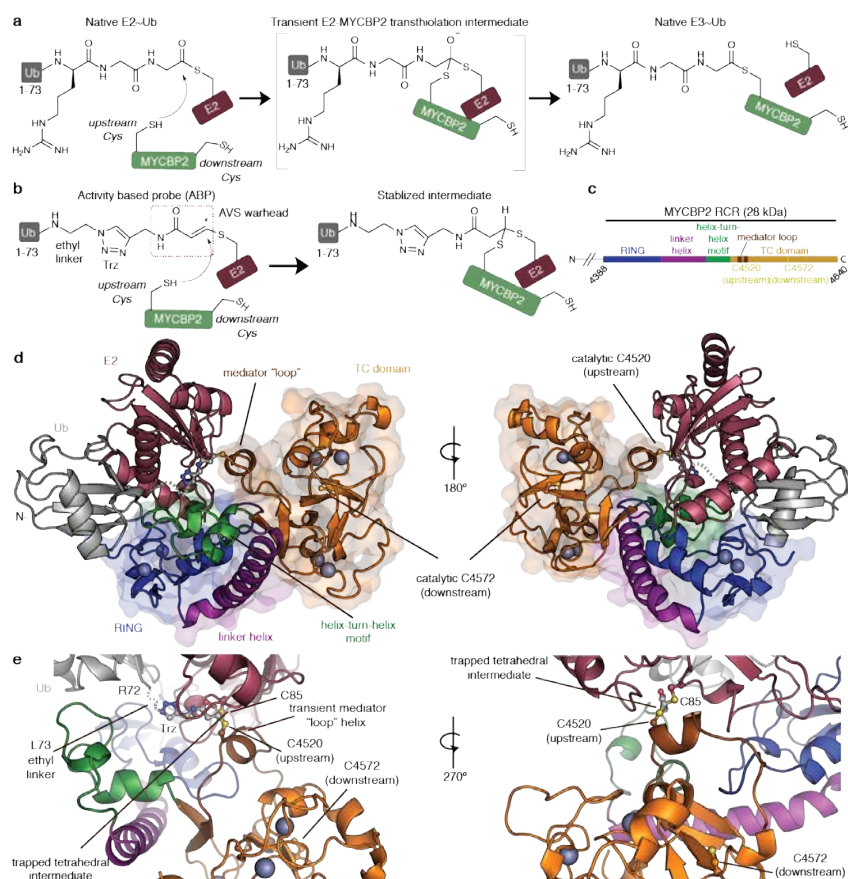


Fig. 1. Stabilization strategy and structure determination of the tetrahedral E2~Ub-MYCBP2 transfer intermediate. **a**, Native mechanism for Ub transfer to the upstream RCR C4520 residue by means of transthioylation with E2~Ub. A transient tetrahedral intermediate is formed prior to intramolecular relay to a downstream cysteine (C4572). **b**, A chemically engineered E2~Ub conjugate acts as an activity-based probe (ABP) and chemically traps the otherwise transient tetrahedral transfer intermediate. ABP design surrogates the final three Ub residues with an ethyl linker, a triazole (Trz) group, and a cysteine-reactive activated vinylsulfide (AVS) warhead. **c**, Domain architecture of the catalytic RCR ligase machinery. **d**, The asymmetric unit consists of a single ternary complex. The RCR machinery in surface representation; RING domain (blue), linker helix (purple), helix-turn-helix (green), TC domain (orange). The trapped tetrahedral Ub transfer intermediate and Trz moiety are depicted in ball and stick. The E2~Ub conjugate is in cartoon representation. The E2 is colored mauve and Ub is gray. **e**, Closeup view of Ub transfer from E2~Ub to the upstream RCR 4520 residue. Upon Ub transfer the otherwise disordered mediator loop adopts an α -helix.

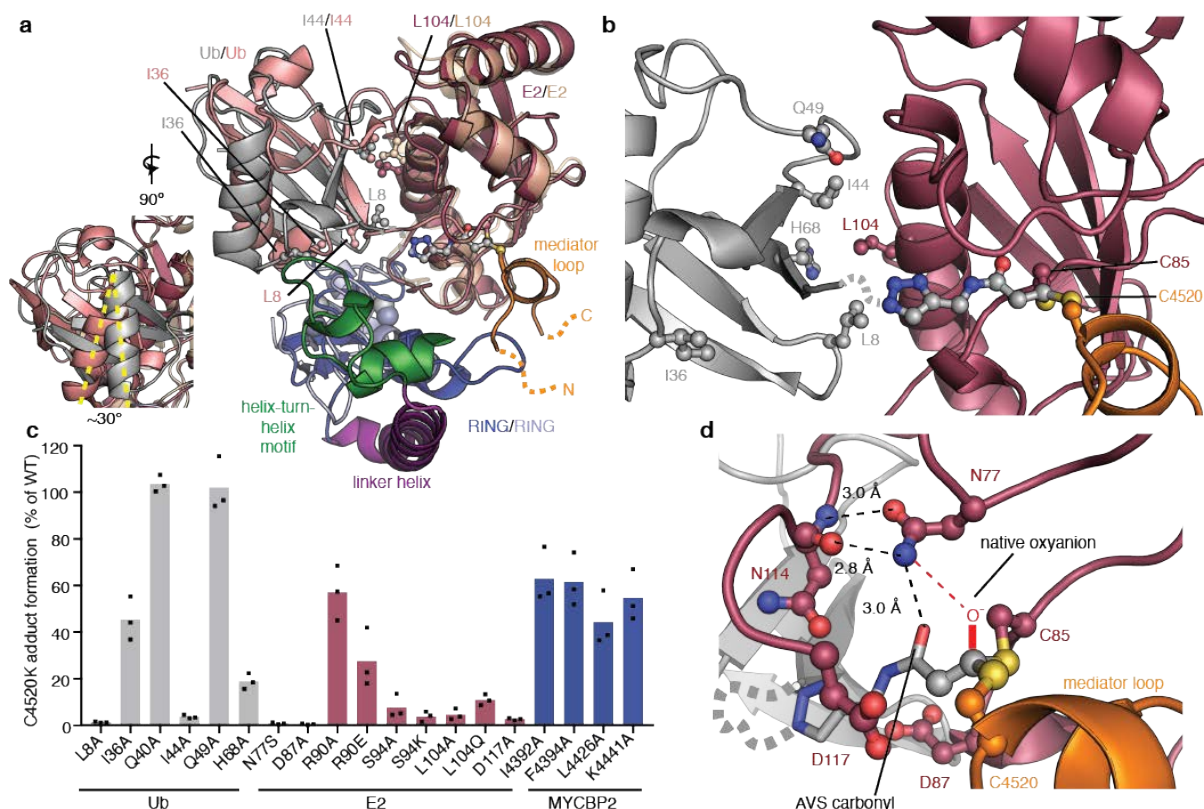


Fig. 2. The RCR engages a closed-like E2~Ub conformation to facilitate exclusive transthiolation to cysteine within a transient helix. **a**, E2 superposition of canonical RNF4:E2~Ub complex (PDB 4AP4) with MYCBP2:E2~Ub complex (TC domain has been omitted). The RNF4 RING is light blue and its bound E2 and Ub components are wheat and light pink⁷, respectively. For the E2~Ub:RCR complex, the tetrahedral crosslink and Trz moiety are depicted in ball and stick. Inset is depicted the crystallographically observed rotation of the Ub molecule. This represents an altered closed-like conformation. **b**, Close up of the interface between the rotated Ub molecule and the E2. **c**, To validate the structure we designed a single turnover E2-E3 isopeptide assay based on a C4520K E3 mutant (Extended Data Fig. 4). Quantification of E2-E3 isopeptide assays ($n = 3$ independent experiments performed with identical purified proteins). Ub Gln40 is proximal to the helix-turn-helix motif but does not form a discernible interaction. Consistent with this, the Gln40Ala mutation has no effect. For representative gel data see Extended Data Fig. 3 c, d. **d**, Close-up view of the engineered, tetrahedral E2~Ub-RCR transthiolation intermediate. The oxyanion, (a proton in our engineered intermediate), has been schematically added to the structure.

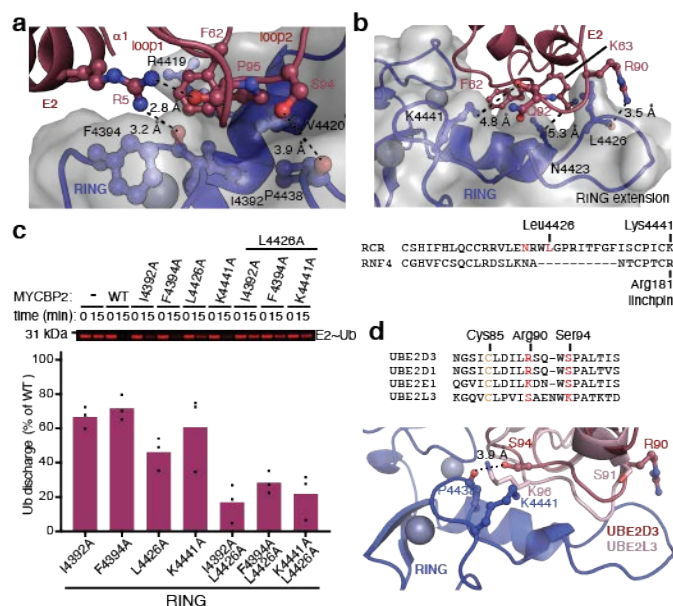


Fig. 3. MYCBP2 RING-E2 interface involves a novel RING extension and specificity determinants. **a**, Canonical RING-E2 interface involving E2 Pro95 engagement with the core of the RING domain. **b**, The canonical interface is supplemented by interactions with the characteristic MYCBP2 RING extension which contacts an E2 region not previously implicated with E2 recognition. This is exemplified by the E2 R90 interaction with MYCBP2 L4426. **c**, Native single turnover E2~Ub discharge assay. Here, E2 is loaded with Ub and reloading is prevented by addition of E1 inhibitor. Discharge of Ub from E2~Ub mediated by addition of MYCBP2 RCR and threonine (50 mM) is monitored. Image is representative replicate with quantification below ($n = 3$ independent experiments performed with identical purified proteins). **d**, E2 sequence alignment highlights difference between MYCBP2 compatible E2s and UBE2L3. Superposition of UBE2L3 (pink; PDB 4Q5E) with UBE2D3 (mauve) from the RCR E2~Ub complex. In the superposition UBE2L3 Ser91 cannot interact with the RCR RING extension and UBE2L3 Lys96 is sterically incompatible when introduced into UBE2D3 (Fig. 2c).

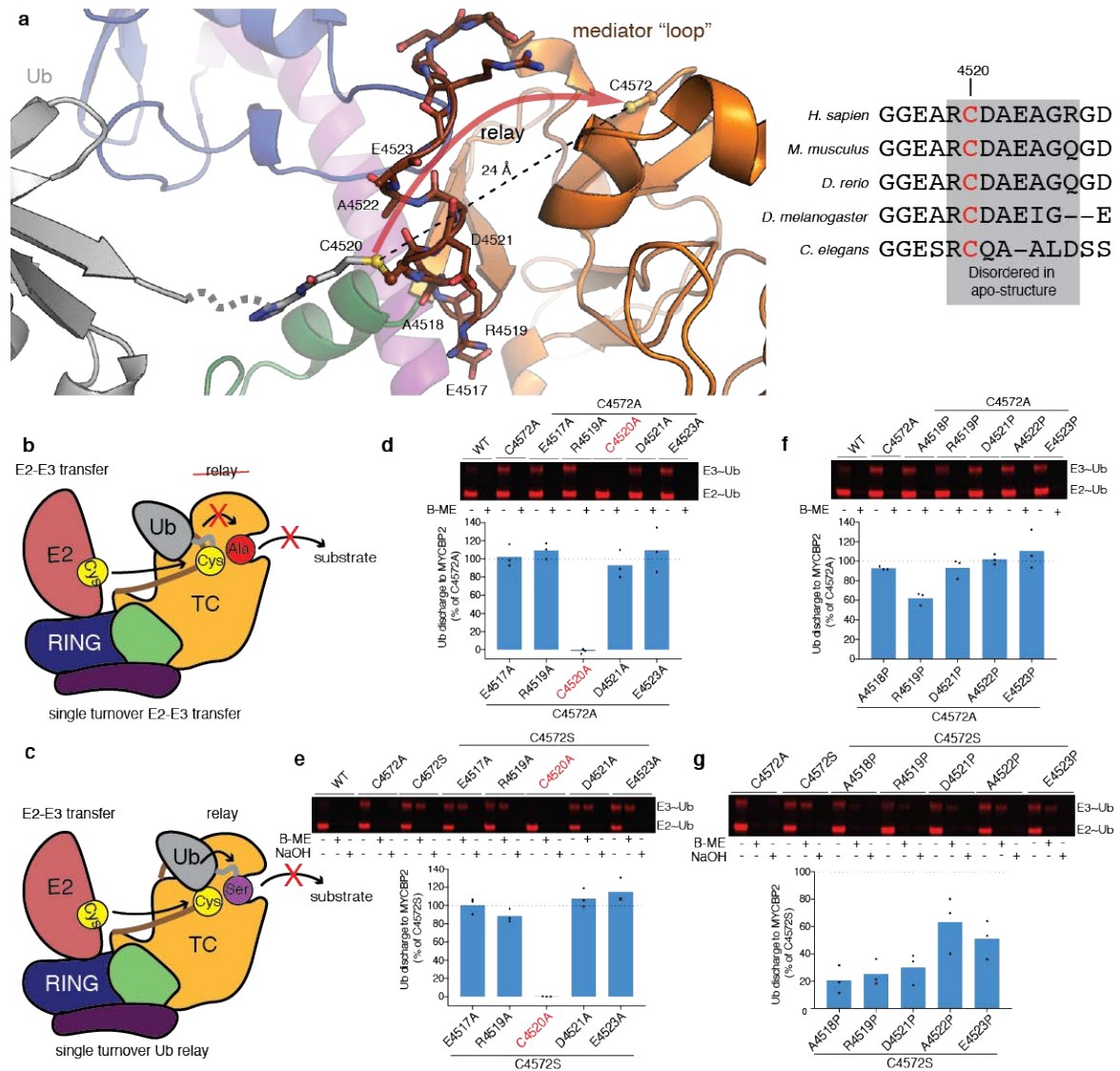


Fig. 4. Alanine and proline scanning of the mediator loop. **a**, Structural rearrangement of the evolutionarily-conserved mediator loop would be required to relay Ub between C4520 and C4572. **b**, Mutation of the downstream cysteine to alanine allows direct assessment of native E2-E3 transthiolation activity. **c**, Mutation of the downstream cysteine to serine restricts RCR activity to the formation of a dead-end ester-linked Ub adduct. For mutants that had negligible effect on E2-E3 transthiolation, reductions in activity can be directly ascribed to Ub relay. **d**, Assessment of alanine scan on E2-E3 transthiolation. B-ME corresponds to 2-mercaptoethanol. **e**, Assessment of alanine scan on Ub relay. **f**, Assessment of proline scan on E2-E3 transthiolation. **g**, Assessment of proline scan on Ub relay. All SDS-PAGE gel images are representative replicates with quantification below ($n = 3$ independent experiments performed with identical purified proteins).

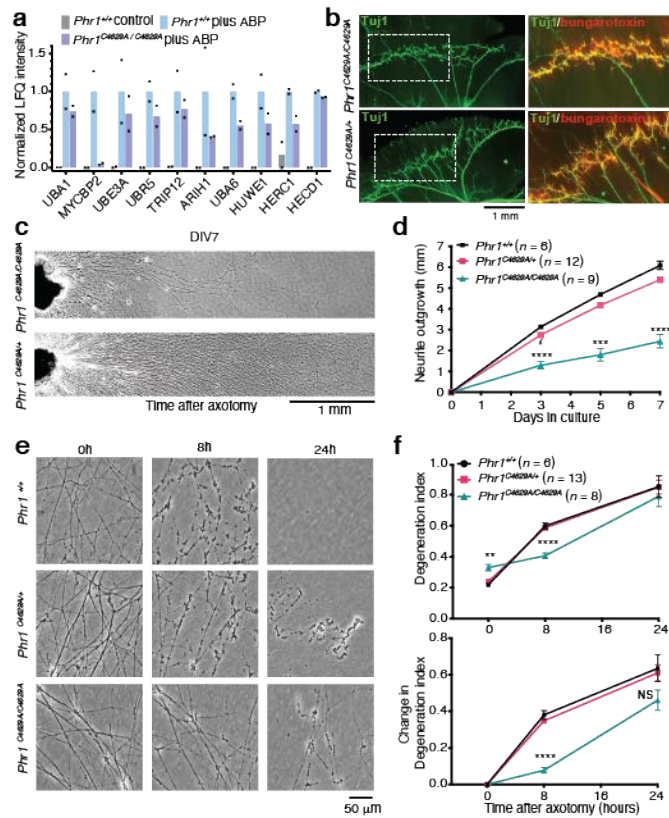


Fig. 5. Neurodevelopmental defects and delayed axotomy-induced axon degeneration in *Phr1*^{C4629A/C4629A} SCG neurons. **a**, Transthiolation activity-based proteomics of E1s and RCR/RBR/HECT E3s in extracted proteomes from MEFs. Signals were normalised to UBA1 ($n=2$ biological replicates). ABP was withheld in the control experiment allowing assessment of non-specific resin binding. **b**, β III-tubulin (Tuj1) immunostaining of the right phrenic nerve terminal branches reveals defective diaphragm innervation in E18.5 *Phr1*^{C4629A/C4629A} embryos. Boxed regions are magnified (right). Acetylcholine receptor (AChR) clusters are labeled by counter-staining with bungarotoxin-TRITC. Representative images from 4 HOM and 9 HET animals. **c**, Representative images of neurite outgrowth at DIV7 in *Phr1*^{C4629A/+} and *Phr1*^{C4629A/C4629A} SCG explant cultures. **d**, Quantification of neurite outgrowth at DIV3-5-7; n numbers per genotype are indicated in the figure (mean \pm SEM; mixed-effects model followed by Tukey post-hoc test). **e**, Representative phase contrast images of neurites from *Phr1*^{+/+}, *Phr1*^{C4629A/+} and *Phr1*^{C4629A/C4629A} SCG explant cultures at the indicated time points after axotomy. **f**, Quantification of the degeneration index in experiments described in (e) from 3 fields per sample; n numbers per genotype are indicated in the figure. Change in degeneration index is also shown (mean \pm SEM; two-way RM ANOVA followed by Tukey post-hoc test). Asterisks indicate: * $P \leq 0.05$, ** $P \leq 0.01$, *** $P \leq 0.001$, **** $P \leq 0.0001$, or NS $P > 0.05$.

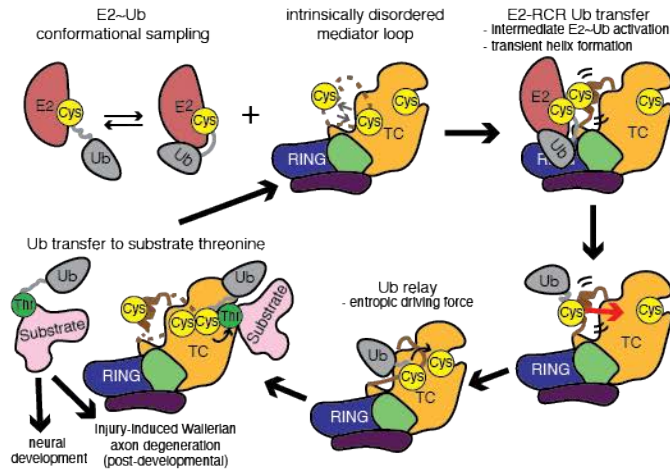


Fig 6. Model for the central role of MYCBP2 RING-Cys-Relay activity in neural development and axon maintenance. The E2~Ub conjugate samples multiple conformations in solution and the mediator loop is unstructured. The RCR machinery in MYCBP2 engages an activated conformation of the E2~Ub conjugate and the mediator loop adopts a transient α -helix whilst undergoing transthiolation. The RING domain serves as an E2 docking site and the TC (tandem cysteine) domain contains both upstream and downstream catalytic cysteines. Upon E2 dissociation, Ub relay to the downstream cysteine is mediated by an entropically driven helix-coil transition. The downstream site is endowed with esterification activity rather than conventional aminolysis activity. Modification of a threonine (Thr) residue in a polypeptide substrate occurs *in vitro* but this remains to be confirmed *in vivo*. Substrate modification is required for normal neural development and programmed axon degeneration in response to injury.

Online Methods

General materials

All DNA constructs generated for this study were verified by DNA sequencing and are available on request through the Medical Research Council Protein Phosphorylation and Ubiquitylation Unit, University of Dundee, reagents website (<https://mrcpppureagents.dundee.ac.uk/>). Chemical probes and mouse line described in this study are available upon request under a material transfer agreement.

Purification and crystallisation of a covalent RCR-UBE2D3-Ub complex.

MYCBP2 residues 4385-4640 were expressed as a GST fusion. Residue numbering for the Uniprot entry for human MYCBP2 (075592) differs as its reannotation has added 38 residues to the protein N-terminus. Following cleavage of the GST tag, MYCBP2 was exchanged by size exclusion chromatography (SEC, Superdex-75) into 20 mM Na₂HPO₄ pH 7.5, 150 mM NaCl, 1 mM TCEP. Ubiquitin (residues 1-73) activity based probe (ABP), containing a thioacrylamide warhead and a UBE2D3 (C21S, S22R, C107S, C111S) recognition element, was prepared as previously described³⁰. ABP (200 μM) and MYCBP2 (50 μM) were exchanged into 20 mM Na₂HPO₄ pH 7.5, 150 mM NaCl and incubated for 4 hr at 30 °C to generate a ternary MYCBP2-UBE2D3-Ub complex. Probe-labelled MYCBP2 was exchanged into 20 mM HEPES pH 7.5, 150 mM NaCl, 1 mM TCEP by SEC. Fractions containing probe-labelled MYCBP2 were pooled and concentrated to 5 mg/mL for crystallisation. Crystals were obtained by vapour-diffusion in 0.85 M sodium citrate, 100 mM sodium chloride, 100 mM Tris-HCl pH 8.0. Single crystals were soaked in mother liquor supplemented with 35% glycerol and vitrified in liquid nitrogen. Data were collected at the European Synchrotron Radiation Facility at Beamline ID29 ($\lambda = 1.2737$ Å). A total of 360° of data were collected with an oscillation range of $\Omega = 0.1^\circ$. Diffraction data were integrated using XDS⁵¹ and scaled using Aimless⁵² (version 0.7.3) from the CCP4 package (version 7.0). Phases were obtained by molecular replacement in Phaser⁵³ (version 2.8.2) using apo-MYCBP2 (PDB 5O6C), UBE2D3 (5EGG), and Ub (PDB 1UBQ) as the search models. Manual model building was carried out with Coot⁵⁴ (version 0.8) and refinement with REFMAC5⁵⁵ (version 5.8.0238). Ramachandran statistics were, favoured: 92.04%, allowed: 6.45%, outliers: 1.51%. Clear electron density for the engineered

bisthioether linkage between UBE2D3 Cys85 and MYCBP2 Cys4520 was visible. To model the linkage a ligand was parameterised using the electronic Ligand Builder and Optimization Workbench (eLBOW) module of the PHENIX suite⁵⁶ (version 1.14). The ligand excluded the ethyl group between Leu73 and the triazole (Trz) as Leu73 was disordered in the structure. The sulphur atoms of Cys85 and Cys4520 were included as part of the ligand. Simulated annealing $2|mFo|-|dFc|$ composite omit maps were generated using the module within the PHENIX suite⁵⁷(version 1.14).

Single-turnover E2 discharge by in-gel fluorescence

Cy3B-labeled ubiquitin was prepared as described previously²⁵. Assays were carried out in Assay Buffer: 20 mM sodium phosphate pH 7.5, 150 mM NaCl, 5 mM MgCl₂, 5 mM ATP. E2 (10 μ M) was charged by E1 (~ 600 nM) with Cy3B-labelled ubiquitin (12.5 μ M) at 37 °C for 30 min then cooled at 23 °C for 3 min. E2 recharging was then blocked by the addition of an E1 inhibitor (MLN4924 derivative, compound 1⁵⁸, (25 μ M)), and further incubated for 10 min. The mixture was then mixed with an equal volume of cleaved MYCBP2 (residues 4378-4640) (5 μ M) and threonine (100 mM) and incubated at 23 °C for the specified time. For MYCBP2 C4520A and RNF4 (residues 1-194)⁷ the final E3 concentrations were 5 μ M and 0.5 μ M, respectively, and lysine concentrations were 0-200 mM. Although efficient lysine discharge was observed with the RCR C4520K mutant, the structural context of this acceptor lysine templates the reaction which can increase the reaction rate by multiple orders of magnitude, thereby reconciling the lack of activity towards free lysine which would be diffusion-limited^{39,59}. For MYCBP2 C4520K mutants, threonine was omitted from the buffer. The reactions were terminated by the addition of 4X LDS loading buffer (Thermo Fisher Scientific) with or without 2-mercaptoethanol. SDS-PAGE gels were scanned with a ChemiDoc MP Gel Imaging System with Image Lab software version 6.0.1 (Bio-Rad Laboratories) and Cy3B fluorescence intensity was quantified using ImageJ version 1.51. Single-turnover Ub-discharge kinetic data were fitted with a one-phase exponential association curve using Prism 7 (Graphpad Software, Inc).

Multiple turnover E2-discharge panel.

Indicated E2s (1 μ M) were incubated in Assay Buffer with MYCBP2 C4520K (5 μ M), Ub (20 μ M), E1 (250 nM), 5 mM ATP.

Mediator loop alanine/proline scanning

Mediator loop mutations were introduced into the C4572A or C4572S backgrounds of MYCBP2. E2 charging with Cy3B ubiquitin was carried out as described for single-turnover E2 discharge by in-gel fluorescence, except E1 was not inhibited. The reactions were terminated by the addition of 4X LDS loading buffer (Thermo Fisher Scientific) (either non-reducing or reducing). For MYCBP2 C4572S ester bond cleavage, 0.14 N NaOH was added and samples were further incubated at 23 °C for 20 min.

Generation of *Phr1*^{C4629A/C4629A} knock-in mice

A C4629A knock-in mutation was created in the *MYCBP2* gene (NCBI transcript NM_207215.2) encoding mouse MYCBP2/Phr1 using CRISPR/Cas9-mediated gene-editing technology (performed by Taconic Biosciences GmbH, Köln, Germany), C57BL/6NTac-Mycbp2em5686(C4626A)Tac. In summary, a guide RNA corresponding to the sequence TGAGGCTCGCTGTGATGCTG was used to target exon 83 of the *Phr1* gene on chromosome 14. This replaced the native cysteine codon (TGT) at position 4629 for an alanine codon. The guide also introduced a single silent mutation immediately upstream thereby introducing an XhoI restriction site for analytical purposes (TGAGGCTCGAGCAGATGCTG). This reduces the codon usage probability for amino acid R4628 from 9.4 % to 6.6 %. Potential F0 founder animals were screened by PCR using extracted biopsies and XhoI positive products were sequenced. Prediction of potential off target sites, revealed that the two closest genes had 3 mismatches. These, together with the next 6 closest matches and two ubiquitin system targets with 4 mismatches (*USP37* and *WWP2*), were PCR screened revealing none were disrupted. Founder mice were backcrossed, and transmission of the *MYCBP2* C4629A was confirmed by direct sequencing of PCR products. Frozen sperm from G1 *MYCBP2* C4629A heterozygous mice was received by the University of Dundee animal facility and used for *in vitro* fertilization of C57BL/6J oocytes, collected from superovulated females. The same 10 potential off-target sites were screened with various primer pairs, and were confirmed to be non-mutated by sequencing. Genotyping of the knock-in allele was routinely performed by

1 PCR using the forward 5'-CACACTTGGAACCCATGC-3' and reverse 5'-
2 ATGACTAGCTTCATGTGTACCCC-3' followed by digestion of the PCR product with
3 XhoI. For a wild type allele, this results in a band of 590 bp while a targeted allele gives a band
4 of 421 bp.

5 Mice were backcrossed on a C57BL/6J (Charles River UK) background for two
6 generations and provided with free access to food (R&M3 pelleted irradiated diet) and water.
7 Animals were kept in individually ventilated cages at 21 °C, 45-65 % relative humidity and a
8 12 h/12 h light/dark cycle under specific-pathogen-free conditions in accordance with UK and
9 European Union regulations. Experiments on mice were approved by the University of Dundee
10 ethical review board under a UK Home Office project license.

11 12 **CRISPR/Cas9-mediated MYCBP2 knock-out of SH-SY5Y cells**

13
14 The MYCBP2 KO SH-SY5Y line was generated using a lentiviral vector,
15 lentiCRISPRv2 (Addgene plasmid # 52961), encoding a single guide RNA scaffold targeting
16 the first exon of MYCBP2 (spacer sequence: GCCTCCGGTAGCGGTCGGCCA). After
17 transduction, cells were initially selected with puromycin, and later subjected to limiting
18 dilution to obtain a homogenous MYCBP2 KO cell population.

19 20 **Primary neuronal cultures**

21
22 SCG explants were dissected from *Phr1*^{+/+}, *Phr1*^{C4629A/+} and *Phr1*^{C4629A/C4629A} littermate
23 E18.5 mouse embryos. Explants were cultured in 35 mm tissue culture dishes pre-coated with
24 poly-L-lysine (20 µg/ml for 1 hr; Sigma) and laminin (20 µg/ml for 1 hr; Sigma) in Dulbecco's
25 Modified Eagle's Medium (DMEM, Gibco) with 1 % penicillin/streptomycin, 50 ng/ml 2.5S
26 NGF (Invitrogen) and 2 % B27 (Gibco). 4 µM aphidicolin (Merck) was used to reduce
27 proliferation and viability of small numbers of non-neuronal cells. Culture media was
28 replenished every 3 days. Neurites were allowed to extend for 7 days before performing the
29 experiments.

30 31 **Acquisition of phase contrast images, neurite outgrowth and axon degeneration assays**

32
33 Phase contrast images were acquired on a DMI8 upright fluorescence microscope
34 controlled with LAS X software (Leica Microsystems) coupled to a monochrome digital

camera (Hamamatsu C4742-95). The objectives used were NPLAN 5X/0.12 for neurite outgrowth assays and HCXPL 20X/0.40 CORR for axon degeneration assays. SCG explants and their extending neurites were captured at low magnification at DIV7. Radial outgrowth was determined by taking the average of two measurements of representative neurite outgrowth for each explant. Measurements were made from overlapping images of the total neurite outgrowth. Axon degeneration assays were performed in the same SCG cultures used for the assessment of neurite outgrowth. Neurites were cut with a scalpel and axon degeneration index⁶⁰, was determined using an ImageJ plugin (<http://rsb.info.nih.gov/ij/download.html>) which calculates the ratio of fragmented axon area over total axon area after binarization of the pictures and subtraction of the background.

Whole-mount immunostaining of diaphragms and branch number quantification

E18.5 mouse embryos were fixed by immersion in 4% (w/v) paraformaldehyde for 24 hours at 4°C. Diaphragms were dissected and washed in phosphate-buffered saline (PBS) before incubation with 10 µg/ml tetramethylrhodamine (TRITC)-conjugated α -bungarotoxin (Thermo Fisher Scientific) for 20 mins at room temperature. Samples were then permeabilized/blocked in PTX (PBS, 0.5% Triton-X100) with 4% BSA (Sigma) for 2 hours at room temperature and incubated overnight at 4 °C with an anti- β III-tubulin (Tuj1) antibody (Sigma, T2200) in blocking solution (1:500 dilution). Following multiple washes in PTX, diaphragms were incubated with an AlexaFluor488-conjugated anti-rabbit antibody (Thermo Fisher Scientific A11008) (1:200 dilution) in blocking solution for 5 hours at room temperature and again extensively washed in PTX. Diaphragms were finally mounted in Vectashield (Vector Laboratories) and images were acquired on a DMI8 upright fluorescence microscope (Leica Microsystems) coupled to a monochrome digital camera (Hamamatsu C4742-95), using a NPLAN 5X/0.12 objective. For quantification of secondary branch number, we traced a parallel line 100 µm below the primary branches, keeping the distance constant across samples. The number of secondary branches that crossed the line were counted.

Mouse Embryonic Fibroblast (MEF) isolation

E12.5 embryos were decapitated, minced, incubated in trypsin-EDTA (Gibco), and pelleted by centrifugation. Cells were resuspended in high glucose DMEM (Gibco) supplemented with 10 % fetal bovine serum (Sigma), 1 mM sodium pyruvate (Gibco), non-essential amino acids (Gibco), 100 U/mL penicillin-streptomycin (Gibco), 2 mM L-glutamine

(Gibco). Cells were then plated in 100 mm dishes, and maintained at 37 °C in 5% CO₂. For proteomics experiments, MEFs were rinsed, scraped manually in Dulbecco's Phosphate-Buffered Saline (DPBS, Gibco), and pelleted by centrifugation. Cells were resuspended in DPBS and pelleted by centrifugation. Cell pellets were snap frozen in liquid nitrogen and stored at -20°C.

NMNAT2-HA expression in mouse embryonic fibroblasts

Mouse embryonic fibroblasts were plated in a 6-well plate at a density of 2 x 10⁶ cells per well. The following day, 1 µg of C-terminal HA-tagged human NMNAT2-coding plasmid, or empty vector, were transiently transfected using Lipofectamine 2000 (Invitrogen) at a Lipofectamine:DNA ratio of 5:1 in Opti-MEM (Gibco). After 24 h, cells were harvested, lysed, and both soluble protein and insoluble proteins were subjected to Western blot analysis. The insoluble fraction was dissolved in 2 % (w/v) SDS prior to addition of 4X LDS sample buffer (Thermo Fisher Scientific).

MYCBP2 probe-labelling for immunoblot analysis

An ABP, containing maltose binding protein (MBP) fused to the N-terminus of a UBE2D3 (C21S, C107S, C111S) and Ub residues 1-73, was prepared as previously described³⁰. To assess MYCBP2 probe labelling, MEF or SH-SY5Y lysates (100 µg) were incubated in lysis buffer (50 mM Tris-HCl pH 7.5, 1 mM EGTA, 1 mM EDTA, 10 mM glycerophosphate, 50 mM sodium fluoride, 5 mM sodium pyrophosphate, 1 mM sodium vanadate, 0.27 M sucrose, 1% NP-40, 0.2 mM PMSF, 1 mM benzamidine, (complete EDTA-free protease inhibitor cocktail (Roche)) with 12 µM MBP-ABP for 4 h at 30 °C. Reactions were terminated by the addition of 4X LDS loading buffer (Thermo Fisher Scientific) containing 2-mercaptoethanol prior to immunoblot analysis.

Immunoblot analysis

Harvested cells were resuspended in lysis buffer with complete EDTA-free protease inhibitor cocktail (Roche). Protein concentration in clarified lysates was assessed using the Bradford method. Samples were prepared in 4xLDS sample buffer (Thermo Fisher Scientific) containing 2-mercaptoethanol. Electrophoresis was performed at 150 V in a NuPAGE 3-8%

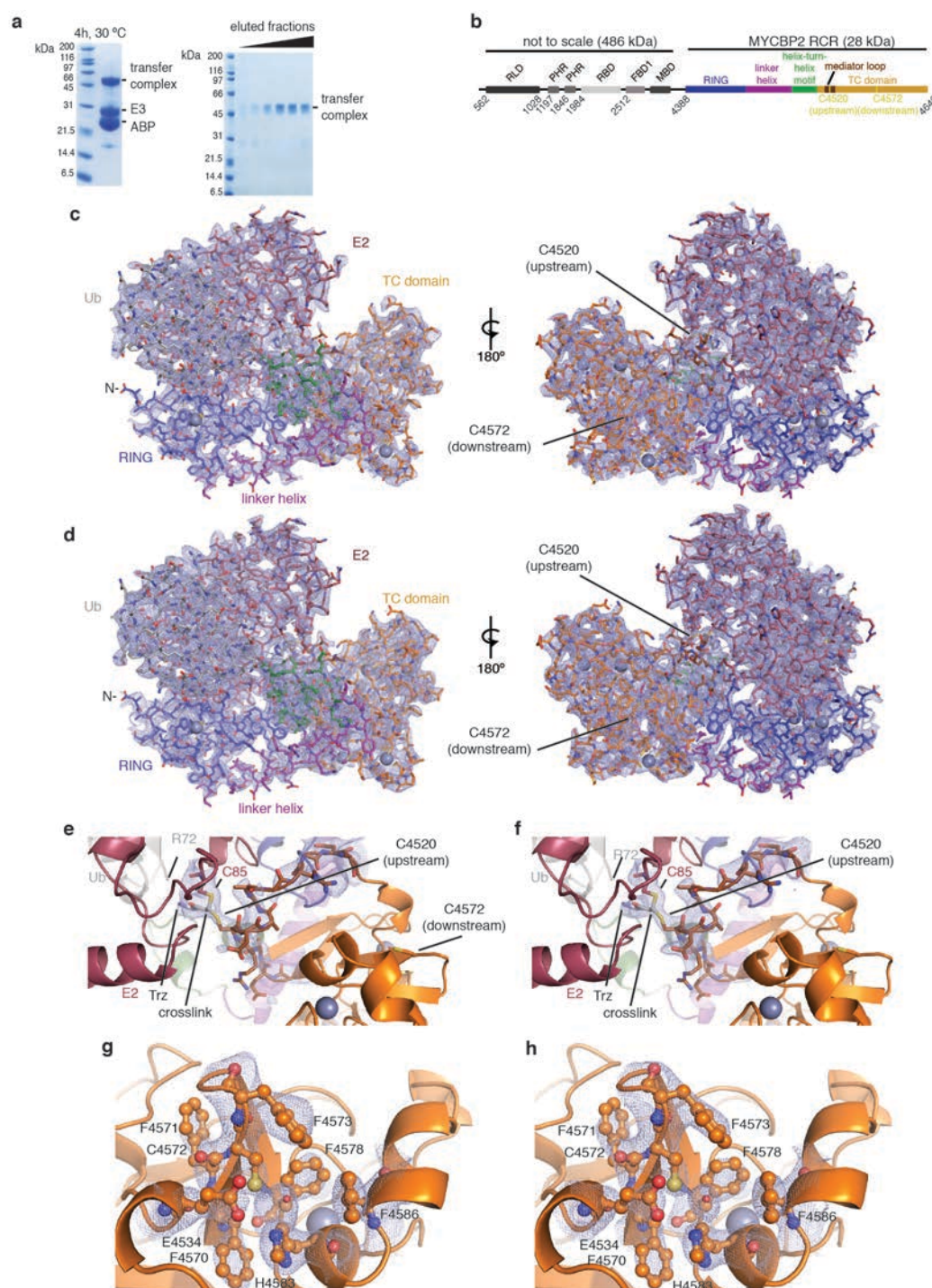
Tris-Acetate gel (Invitrogen) when blotting for MYCBP2 or a NuPAGE 4-12% Bis-Tris gel (Invitrogen) for NMNAT2-HA. Following electrophoresis proteins were transferred to PVDF membrane. Membranes were blocked in TBS-T (10 mM Tris-HCl pH 7.4, 150 mM NaCl, 0.05% Tween-20) containing 5% (w/v) non-fat dried skimmed milk powder for 1 h before incubation with commercially available primary antibody (MYCBP2 Abcam Ab86078 1:10,000 dilution, HA tag 3F10 Sigma 27573500 1:2500 dilution, Vinculin Abcam Ab129002 1:2500 dilution, Tubulin ProteinTech 66031 1:10,000 dilution) or a previously described antibody raised against the RCR domain (anti-MYCBP2 SA357 aa4378-4640²⁵ 1:1200 dilution). After washing in TBST-T, membranes were incubated for 45 min in secondary HRP-coupled antibody (anti-Rabbit Cell Signaling Technology 7074S 1:5000 dilution, anti-Rat Cell Signaling Technology 7077S 1:5000 dilution, anti-Sheep Invitrogen 31480 1:5000, or anti-Mouse Cell Signaling Technology 7076S, 1:5000 dilution). Membranes were then washed before adding the chemiluminescent substrate (ECL Prime Sigma, for ABP-labelling experiment and NMNAT2-HA; ECL Thermo Fisher Scientific, for MYCBP2 and Tubulin), and exposing to radiographic film.

Activity-based proteomics

MEFs from WT and homozygote genotypes were rinsed and collected with ice-cold PBS, and extracted with ice-cold lysis buffer 2 (50 mM Tris-HCl pH 7.5, 10 mM sodium 2-glycerophosphate, 50 mM sodium fluoride, 5.0 mM sodium pyrophosphate, 1.0 mM sodium orthovanadate, 0.27 M sucrose, 50 mM NaCl, 0.2 mM (PMSF), 1.0 mM benzamidine, 10 μ M TCEP, 1% NP-40) on ice for 20 min. Protein concentration in clarified lysates was determined by Bradford assay and concentrations normalised across genotypes. Biotin-labelled E3 activity-based probe with a UBE2D3 recognition element and Ub residues 1-73²⁵ was added to lysates at 10 μ M and incubated at 30°C for 4 hr. Biotin enrichment was then carried out against streptavidin resin followed by on-resin tryptic digestion and LC-MS/MS analysis²⁵. Data were processed using LFQ quantification with MaxQuant (<http://www.maxquant.org>). To facilitate graphical depiction, the vast dynamic range of LFQ intensities were normalised to the mean UBA1 signal in ABP-treated wild-type MEFs. UBA1 is the predominant ubiquitin E1 and yields a relatively high ABP signal and it was assumed that levels were similar across all genotypes.

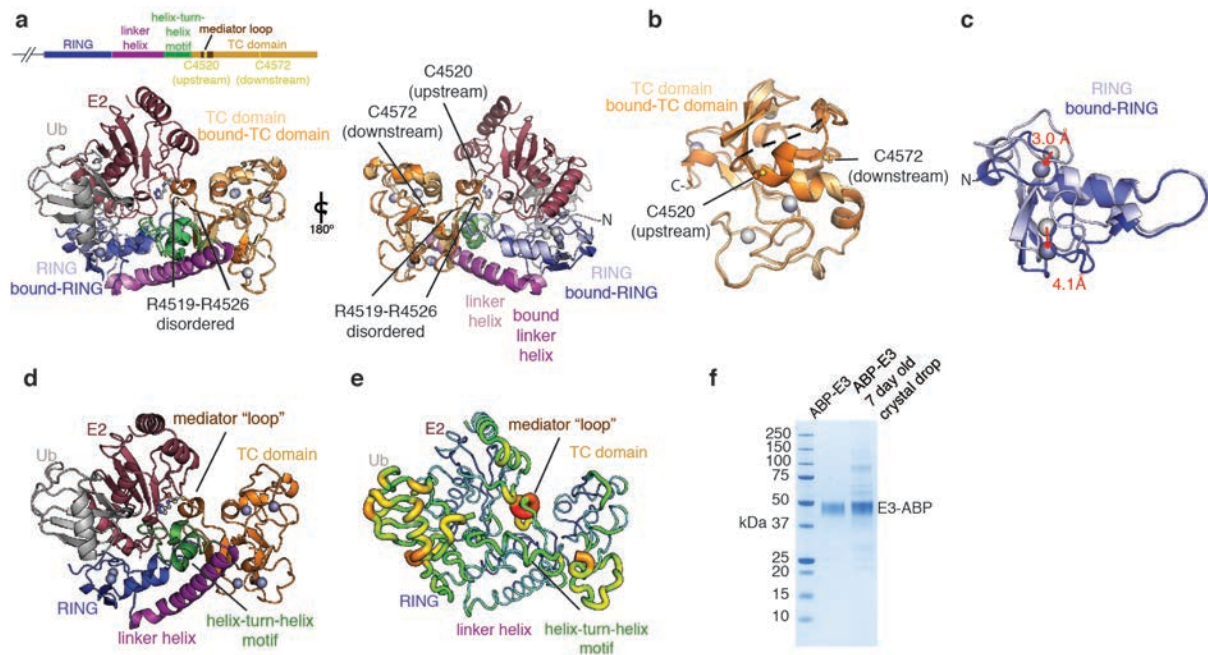
Data availability

Protein Data Bank coordinates and structure factors for RCR-E2-Ub have been deposited with accession code 6T7F. All DNA constructs were verified by DNA sequencing and are available through the Medical Research Council Protein Phosphorylation and Ubiquitylation Unit, University of Dundee, reagents website (<https://mrcppureagents.dundee.ac.uk/>). The data that supports these findings, including raw mass spectrometry and microscopy data, are available from the corresponding author upon request s.s.virdee@dundee.ac.uk.



Extended Data Fig. 1. Structure determination and representative views of the E2~Ub-MYCBP2 transfer intermediate. **a**, A crosslinked transfer complex was prepared by incubating ABP (200 μ M) and E3 (MYCBP2 RCR) (50 μ M) for 4 h at 30 °C. Complex formation was assessed by SDS-PAGE (left). The stabilized transfer complex was purified by size-exclusion chromatography (right). **b**, Domain architecture of MYCBP2 including the catalytic RCR machinery. **c**, The RCR machinery is in stick representation; RING domain (blue), linker helix (purple), helix-turn-helix (green), TC domain (orange), mediator loop (brown), E2 (mauve) and Ub (gray). The mesh represents a simulated annealing composite omit $2|mFo|-|dFc|$ electron density map contoured at 1.0 σ . **d**, As above except the mesh represents the experimental $2|Fo|-|Fc|$ electron density map contoured at 1.0 σ . **e**, Close-up view of the three-way crosslink between E2 C85, RCR C4520 and the Ub carboxy terminus.

The mesh represents a simulated annealing composite omit $2|mFo|-|dFc|$ electron density map contoured at 1.0σ carved around the mediator loop G4515 – D4529, E2 residues C85, and the crosslink. **f**, As **e** except the mesh represents the experimental $2|Fo|-|Fc|$ electron density map contoured at 1.0σ . **g**, Close-up view of the Ub-esterification site, in the apo-structure the esterification site is occupied by a Thr residue due to crystal packing. The mesh represents a simulated annealing composite omit $2|mFo|-|dFc|$ electron density map contoured at 1.0σ carved around E4534, F4570 – F4573, H4583, F4586 and an ordered water molecule. **h**, As **g** except the mesh represents the experimental $2|Fo|-|Fc|$ electron density map contoured at 1.0σ .



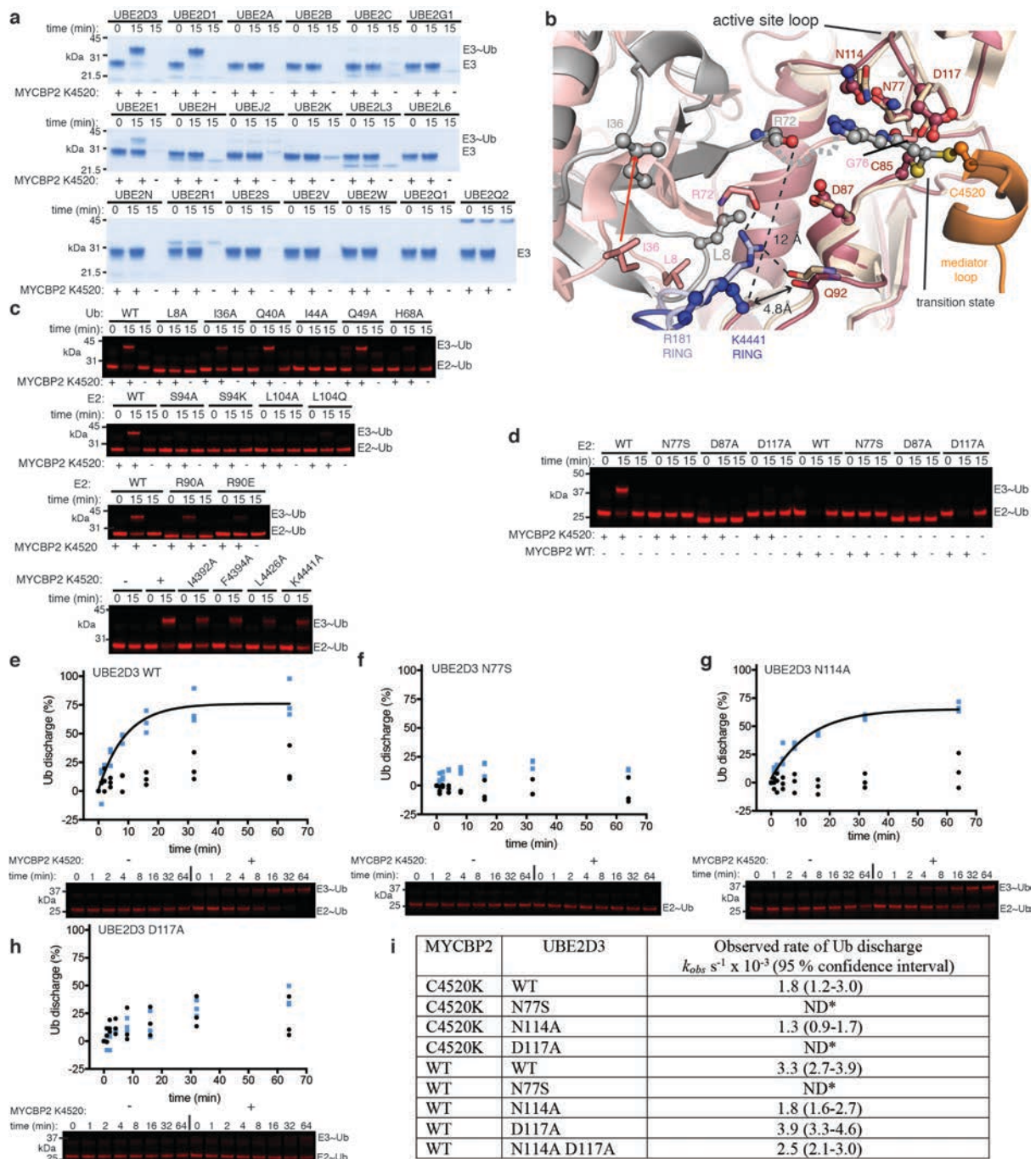
Extended Data Fig. 2. Superposition of apo-MYCBP2 (PDB 5O6C), E2~Ub bound-MYCBP2 and protein crystal stability. **a**, Apo-MYCBP2 residues Asn4379-His4638 were aligned with bound-MYCBP2 residues Asp4387-Asn4636. The RCR, E2 and Ub are in cartoon representation: Coloring (apo-MYCBP2/bound-MYCBP2) zinc ions (light gray/gray), RING domain (light blue/blue), linker helix (pink/purple), helix-turn-helix (light green/green) and tandem cysteine domain (yellow/orange). In the apo structure, 8 residues from the mediator loop are disordered and are represented by a black dashed line. The E2 is colored mauve and Ub is gray. MYCBP2 Residues Ala4518, Gly4527, Cys4520 and Cys4572 are in ball and stick representation. In the bound-MYCBP2 structure E2 residue C85 and the engineered crosslinker are in ball and stick representation. **b**, Closeup of TC domains, in the E2~Ub bound structure the eight mediator loop residues, that were disordered in the apo structure, adopt a helical conformation in the E2~Ub:RCR transfer complex. **c**, Closeup of RING domains, in the E2~Ub bound structure the RING domain has twisted towards the linker-helix this results in a 3.0 and 4.1 Å shift of Zn^{2+} 1 and Zn^{2+} 2, respectively. **d**, Representative view of the E2~Ub-MYCBP2 transfer intermediate. **e**, Representative view of the E2~Ub-MYCBP2 transfer intermediate colored by B-factors (blue thin-cartoon lowest B-factors to red thick-cartoon highest B-factors) indicates that ubiquitin and the mediator loop are the most disordered components of the complex. **f**, SDS-PAGE gel of purified ABP-MYCBP2 complex and ABP-MYCBP2 complex recovered from a crystal drop containing the productive conditions (0.85 M sodium citrate, 100 mM sodium chloride, 100 mM Tris-HCl pH 8.0). The ABP-labelled transfer complex is stable during crystallization. Experiment was repeated twice with similar results.

MYCBP2 -UBE2D3- Ub	
Data collection	
Space group	H3 ₂
Cell dimensions	
<i>a</i> , <i>b</i> , <i>c</i> (Å)	179.01, 179.01, 87.28
α, β, γ (°)	90, 90, 120
Resolution (Å)	48.6 - 2.58 (2.69 - 2.58)*
<i>R</i> _{merge}	0.103 (2.70)
<i>I</i> / σ <i>I</i>	20.7 (0.9)
CC (1/2)	0.99 (0.434)
Completeness (%)	98.3 (91.4)
Redundancy	17.6 (9.1)
Refinement	
Resolution (Å)	48.6 - 2.58 (2.69 - 2.58)
No. reflections	15778
<i>R</i> _{work} / <i>R</i> _{free}	0.202/0.265
No. atoms	
Protein	3717
Ligand/ion	13/6
Water	41
<i>B</i> -factors	
Protein	79.92
Ligand/ion	125.43/ 62.16
Water	62.73
R.m.s. deviations	
Bond lengths (Å)	0.01
Bond angles (°)	1.58

Values are for a single crystal

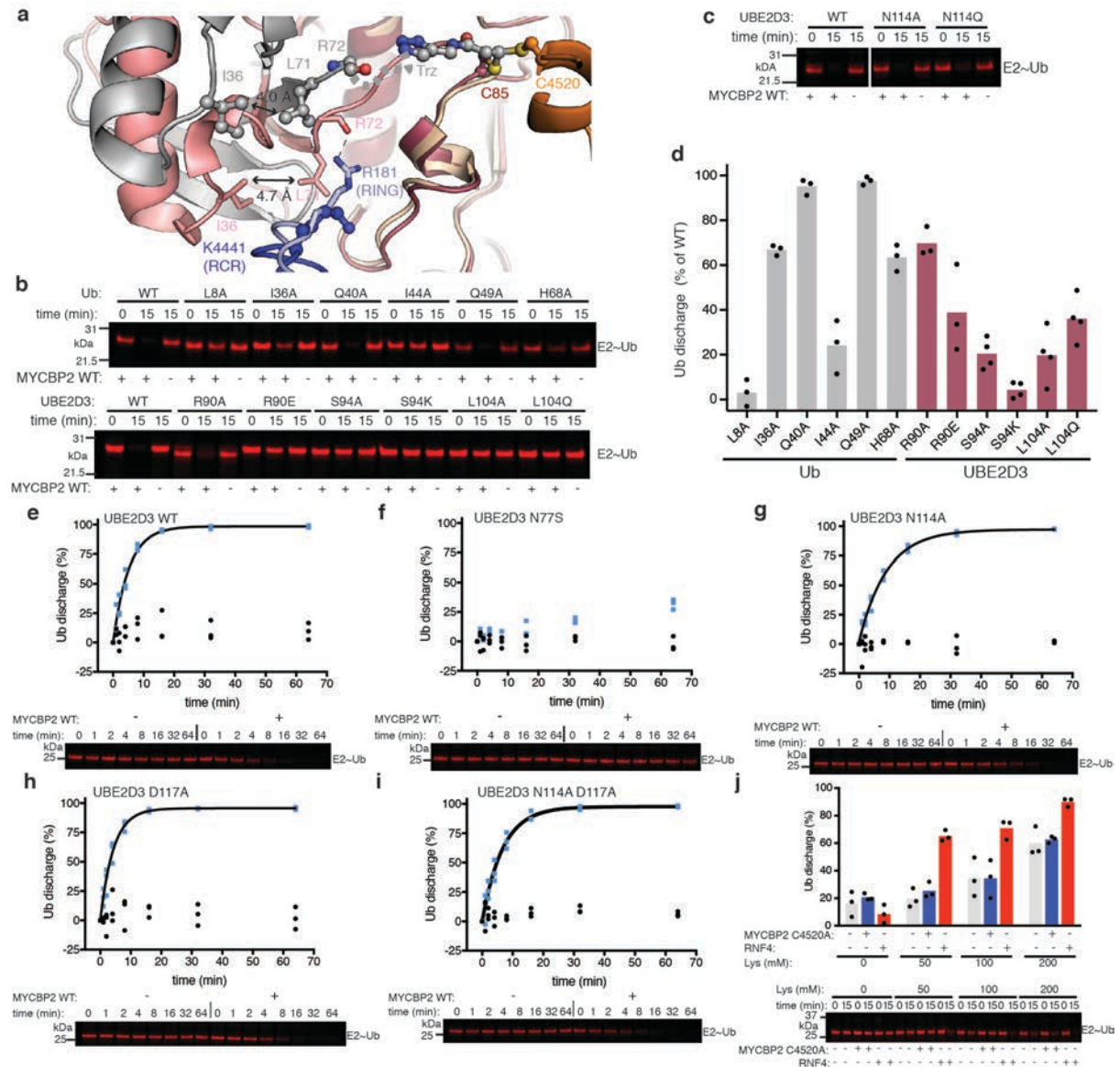
*Values in parentheses are for highest-resolution shell.

Extended Data Fig. 3. Data collection and refinement statistics. Crystallographic data were collected from a single crystal.



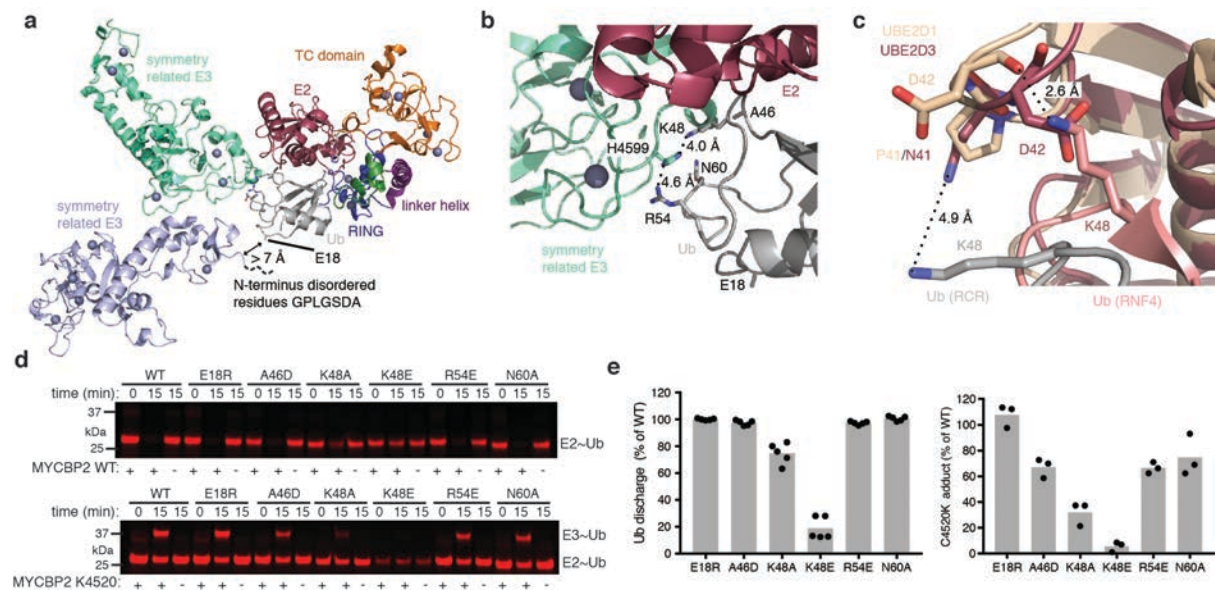
Extended Data Fig. 4. Mutational analysis of E2-E3 Ub transfer was determined by single-turnover isopeptide formation in the context of an RCR C4520K mutant. To decouple E2-E3 Ub transfer (what our structure is reflective of) from subsequent relay and substrate esterification, we devised a robust assay that results in transfer of Ub from E2 to a dead-end product. To achieve this, we mutated the upstream Cys4520 residue to a lysine (Cys4520Lys). We found Ub was transferred to the lysine forming a stable isopeptide adduct. **a**, Activity was efficient and only E2's previously shown to support MYCBP2 E3 activity supported isopeptide bond formation²⁵. Experiment was repeated twice with similar results. **b**, A subset of hallmark interactions involved in closed E2~Ub stabilization are maintained (coloring as Fig. 2a). **c**, Representative replicate from single-turnover E2~Ub isopeptide assay used for quantification presented in Fig. 2c (also see methods). **d**, The majority of mutants were also tested with wild type MYCBP2 in multiple turnover threonine-discharge assays (Extended Data Fig. 5), which yielded similar activity profiles. However, one exception was with E2

mutation D117A. Whereas D117A was fully active with MYCBP2 WT, it was completely inactive in C4520K isopeptide formation. This is reflective of this residue having a lysine-specific role that is redundant with native MYCBP2 E2-E3 transthiolation. **e-h**, Kinetic analysis for E2 active site residues ($n = 3$ independent experiments performed with identical purified proteins). Blue squares and black circles correspond to experiments where E3 was added or withheld, respectively. E2 reloading was blocked by addition of E1 inhibitor and depletion of the E2~Ub species was quantified. **i**, Observed rates of single-turnover Ub discharge (k_{obs}) from experiments **e-h**. Observed rate constants were obtained from the one-phase exponential association equation using the routine within Graphpad Prism. Assays were carried out in triplicate using identical purified proteins. The 95 % confidence intervals for k_{obs} are presented. ND* indicates that rates of Ub discharge in the presence of E3 were indistinguishable from background E2~Ub hydrolysis. Observed rates for native transthiolation activity determined from experiments presented in Extended Data Fig. 5 are also tabulated.



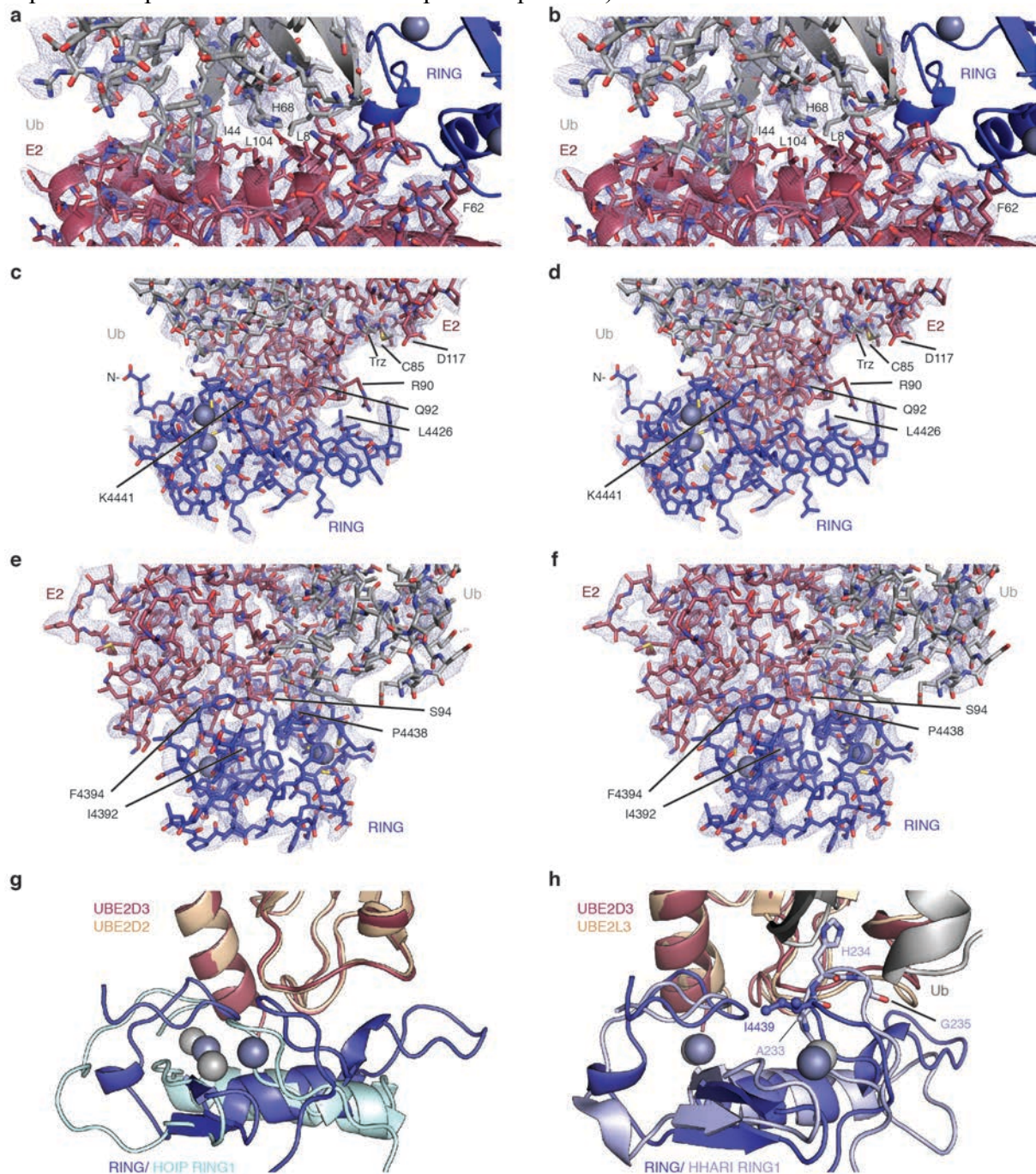
Extended Data Fig. 5. Mutational assessment of native MYCBP2 E2-E3 transthiolation activity and demonstration of attenuated E2~Ub reactivity. a, Proposed intramolecular role for Ub I36 in maintaining a closed-like E2~Ub conformation. The interaction between Ub I36 and L71 is maintained in the “closed-like” E2~Ub conformation. Superposition of the RCR

E2~Ub and RNF4 E2~Ub (PDB 4AP4) complexes. The gap between Ub I36 and L71 has decreased by 0.7 Å in the RCR complex. The RCR, E2 and Ub are in cartoon representation with select residues in ball and stick representation: Ub I36, L71, R72 and the engineered linker (gray), E2 C85 (mauve), RCR K4441 (blue) and C4520 (orange). The RNF4 E2~Ub complex is in cartoon representation with select residues in stick representation: Ub I36, L71, R72 (pink), R181 (purple). **b**, For the selected mutants, MYCBP2 activity was assessed using single turnover E2~Ub discharge assays mediated by the presence of wild type MYCBP2 and threonine (50 mM). **c**, Single turnover E2~Ub discharge assay mediated by the presence of wild type MYCBP2 and threonine (50 mM) for E2 Asn114Ala and Asn114Gln mutants. Experiment repeated twice with similar results. **d**, Quantification for selected mutants, ($n = 3$ -4 independent experiments performed with identical purified proteins). **e-i** native single-turnover WT MYCBP2 and threonine dependent E2~Ub discharge assay. Observed rate constants tabulated in Extended Data Fig. 4 were obtained from the one-phase exponential association equation using the routine within Graphpad Prism. Blue squares and black circles correspond to experiments where E3 was added or withheld, respectively. ($n = 3$ independent experiments performed with identical purified proteins) **j**, Quantification of lysine discharge assay in the presence of a transthiolation-defective RCR A4520 mutant or the canonical RING E3 RNF4 ($n = 3$ independent experiments performed with identical purified proteins). Although efficient lysine discharge was observed with the RCR C4520K mutant, the structural context of this acceptor lysine templates the reaction which can increase the reaction rate by multiple orders of magnitude, thereby reconciling the lack of activity towards free lysine which would be diffusion-limited^{39,59}.



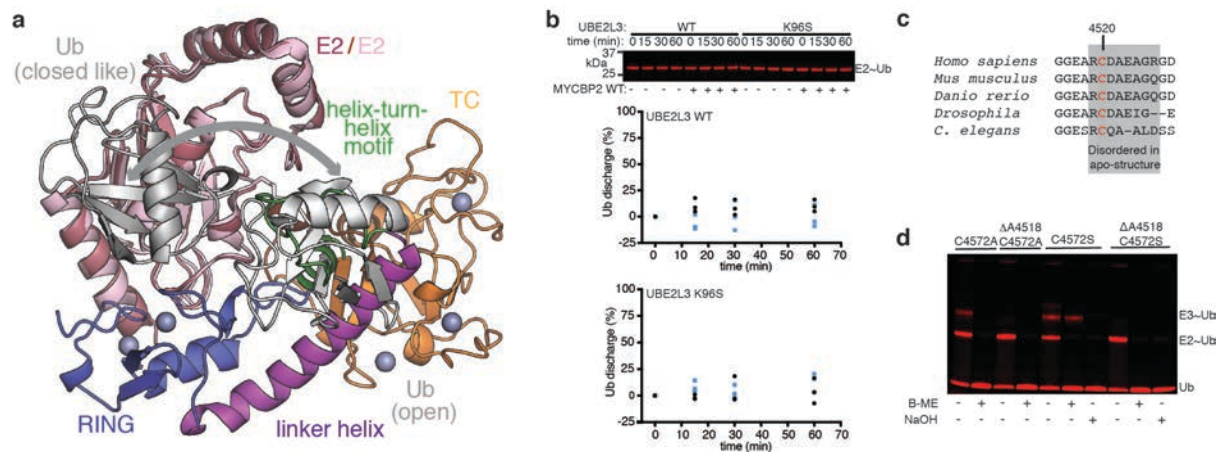
Extended Data Fig. 6. Consideration of crystal packing effects on adoption of the closed like E2~Ub conformation and assessment of their significance in solution. **a**, Interface between Ub (gray), E2 (mauve) RCR (TC domain, orange; linker helix, purple; helix-turn-helix, green; RING, blue) and two symmetry-related RCR molecules (cyan and light-blue). The side chain of Ub E18 and the first 7 residues of the RCR construct are disordered. **b**, Closeup of the interface between Ub, E2 and symmetry related E3. Ub K48 and R54 are in close proximity to symmetry related MYCBP2 H4599. **c**, Superposition of the RCR E2~Ub and RNF4 E2~Ub (PDB 4AP4) complexes highlighting the position of Ub Lys48. The altered Ub packing in the RCR complex (E2, mauve; Ub, gray) results in Ub Lys48 shifting away from E2 D42, relative to the RNF4 complex (E2 wheat; Ub, pink). **d**, Single-turnover E2~Ub discharge and single-turnover isopeptide formation for the indicated Ub variants. The Ub

E18R, A46D, R54E, and N60A mutants were discharged similarly to WT Ub, suggesting that the interface with a second copy of MYCBP2 does not exist in solution or is not required for activity. The Ub K48A and K48E mutants reduced activity, which would not be expected if the interaction with H4599 residue within the symmetry related MYCBP2 contributed to prevention of a canonical closed-conformation in solution. As K48 is proximal to the E2 it seems more likely that it intrinsically contributes to closed and closed-like activation. **e**, Quantification of single-turnover E2~Ub discharge ($n=5$ independent experiments performed with identical purified proteins) and single-turnover isopeptide formation ($n=3$ independent experiments performed with identical purified proteins).



Extended Data Fig. 7. Representative electron density centered on key E2~Ub-RING interfaces and comparison with E2~Ub-RING1 interfaces. **a**, The E2-Ub interface is centred on E2 L104, Ub L8, I44, H68, and V70. E2 (mauve) and Ub (gray) are shown as sticks, the RCR RING domain (blue) is shown as a cartoon. For clarity RCR regions C-terminal of

the RING are not shown. The mesh represents a simulated annealing composite omit $2|mFo|-|dFc|$ electron density map contoured at 1.0σ . **b**, As **a** except the mesh represents the experimental $2|Fo|-|Fc|$ electron density map contoured at 1.0σ . **c**, View of the RING-E2 interface, RCR RING (blue), E2 (mauve) and Ub (gray) are shown as sticks. The RCR equivalent to the ‘linchpin’ residue (K4441) and the functionally important RING extension residue (L4426) are labelled. The mesh represents a simulated annealing composite omit $2|mFo|-|dFc|$ electron density map contoured at 1.0σ . **d**, As **c** except the mesh represents the experimental $2|Fo|-|Fc|$ electron density map contoured at 1.0σ . **e**, View of the RING-E2 interface focused on RCR residues L4392, F4394 and the interaction between E2 S94 and RING P4438. The mesh represents a simulated annealing composite omit $2|mFo|-|dFc|$ electron density map contoured at 1.0σ . **f**, As **e** except the mesh represents the experimental $2|Fo|-|Fc|$ electron density map contoured at 1.0σ . **g**, Superposition of MYCBP2 E2~Ub and HOIP E2~Ub complexes (PDB 5EDV) highlighting the shift in E2 binding site for HOIP RING1 (E2s were superposed). MYCBP2 complex RING (blue), E2 (mauve), zinc ions (gray); HOIP complex RING1 (cyan), E2 (wheat), zinc (light gray). **h**, Superposition of MYCBP2 E2~Ub and HHARI E2~Ub complexes (PDB 5UDH) highlighting a loop insertion in HHARI RING1 that prevents the closed E2~Ub conformation. HHARI His234 would sterically clash with Ub in the “closed” E2~Ub, and similarly, His234 is incompatible with the “closed-like” E2~Ub adopted in the RCR complex. MYCBP2 complex RING (blue), E2 (mauve), Ub (gray), zinc (gray); HHARI complex RING1 (light blue), E2 (wheat) and zinc (light gray).



Extended Data Fig. 8. The RCR-helix-turn-helix motif prevents binding of an open E2~Ub conjugate, UBE2L3 activity cannot be imparted by Lys96Ser mutation, and further mediator loop analysis. **a**, Superposition of ‘open’ conformation E2~Ub from a HECT E2~Ub complex (PDB 3JVZ) with the RCR E2~Ub complex. The open conformation in the HECT E2~Ub complex is incompatible with the observed RCR conformation as Ub is sterically blocked by the helix-turn-helix motif. HECT E2 (pink) and Ub (light gray) are displayed in cartoon representation. **b**, Despite introduction of the corresponding lysine residue into UBE2D3 abolishing its activity, we could not impart UBE2L3 activity by substitution of Lys96 to Ser, as found in UBE2D3. Blue squares and black circles correspond to experiments where E3 was added or withheld, respectively (n = 3 independent experiments performed with identical purified proteins). **c**, The mediator loop has high sequence conservation across orthologues. The deletions in *Drosophila* and *C. elegans* relative to human MYCBP2 imply the Ub relay process is highly plastic. **d**, Deletion of mediator loop residue A4518 substantially impairs E2-E3 transthiolation and Ub relay. Experiment was repeated twice with similar results.

a

E3		E2		Distance (Å)	PDB
MYCBP2	Pro4438	UBE2D3	Ser94	3.9	
TRAF6	Pro107	UBE2N	Ser96	3.0	5VNZ
cIAP2	Pro589	UBE2D2	Ser94	3.0	3EB6
RNF45	Pro376	UBE2G2	Ser111	2.9	4LAD
FANCL	Pro360	UBE2T	Ser101	2.8	4CCG
RING1B	Pro88	UBE2D3	Ser94	2.7	4S3O
AO7	Pro199	UBE2D2	Ser94	2.7	5D1K
Mdm2	Pro476	UBE2D2	Ser94	2.6	5MNJ
c-CBL	Pro409	UBE2D2	Ser94	2.6	4A49
RNF165	Pro332	UBE2D2	Ser94	2.6	5D0K
TRIM25	Pro51	UBE2D2	Ser94	2.6	5FER
ZNRF1	Pro222	UBE2N	Ser96	2.6	5YWR
RNF38	Pro451	UBE2D2	Ser94	2.5	4V3L
RNF4	Pro243	UBE2D1	Ser94	2.5	4AP4
BIRC7	Pro283	UBE2D2	Ser94	2.5	4AUQ
TRIM23	Pro73	UBE2D2	Ser94	2.4	5VZW
cNot4	Pro75	UBC4	Ser95	2.3	5AIE

b

*

MYCBP2	FISC P ICKNK
TRAF6	GHK C PVDNEI
cIAP2	LRK C PICRST
RNF45	DTSC P TCRMS
FANCL	FGE C PYCSKP
RING1B	NKE C P T CRKK
AO7	GVQ C PVCREP
Mdm2	NKP C PVCRQP
c-CBL	GQG C PFRCCE
RNF165	SKK C PICRVD
TRIM25	PYL C PQCRV
ZNRF1	NRSC P EHFAD
RNF38	NRTC P ICRAD
RNF4	ANT C P T CRKK
BIRC7	LQL C PICRAP
TRIM23	AIRC P FDQV
CNOT4	NGL C PACRKP

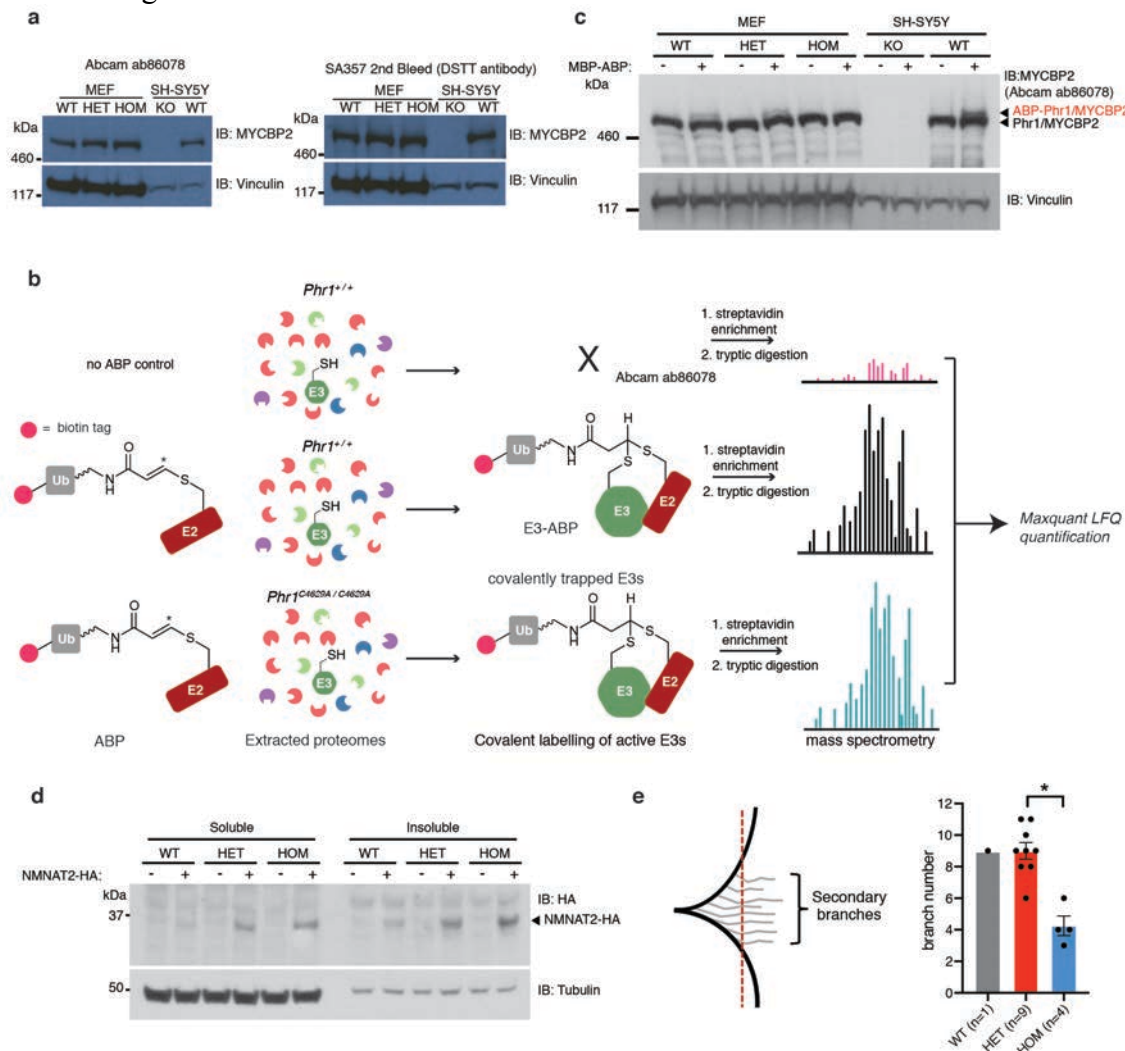
c

E3		E2		Distance (Å)	PDB
MYCBP2	Pro4438	UBE2D3	Ser94	3.9	
HOIP	Pro745	UBE2D2	Ser94	4.3	5EDV
HHARI	Pro232	UBE2L3	Lys96	5.5	5UDH
HHARI	Pro232	UBE2L3	Lys96	6.4	5TTE
Bd PARKIN	Pro325	UBE2L3	Lys96	6.9	6DJW

d

MYCBP2	FISC P ICKNK
HOIP	DMV C PACGRP
HARRI	TKE C PKCHVT
Bd PARKIN	TL P C P AGCEN

Extended Data Figure 9. Relaxation of the E2 Ser94-RING Pro4438 interaction is crystallographically observed for RING-linked E3s (RBRs and RCR) relative to canonical RINGs. Interestingly, the Ser94-Pro4438 H-bond is highly conserved in solved E2-RING structures but for canonical RING E3s an idealized geometry is observed (2.3-3.0 Å). For RBR E3s that undergo transthiolation, this H-bond distance is comparable to that observed for the RCR being ~0.4 Å longer. Thus, it would appear that relaxation of this H-bond may be a hallmark of RING-linked E3s but the mechanistic basis for this is not clear. **a**, Distances between E2 Ser94 (gamma oxygen) and E3 Pro (carbonyl oxygen) for MYCBP2 relative to canonical RING E3s. **b**, Alignment of the C-terminal portion of the RING including the 7th and 8th zinc coordinating residues. The conserved proline that interacts with E2 serine 94 is shown in blue. Zinc coordinating residues are shown in red. The linchpin residue location is indicated with an asterisk. **c**, Distances between E2 Ser94 (gamma oxygen), or E2 Lys96 (epsilon amino nitrogen), and E3 Pro (carbonyl oxygen) for MYCBP2 relative to RBR E3s. **d**, Alignment of the c-terminal portion of the RING including the 7th and 8th zinc coordinating residues. The conserved proline that interacts with E2 serine 94 in MYCBP2 shown in blue. Zinc coordinating residues are shown in red.



Extended Data Figure 10. Further characterization of *Phr1*^{C4629A/C4629A} mouse line. **a, Expression levels of Phr1/MYCBP2 in *Phr1*^{+/+} (WT), *Phr1*^{C4629A/+} (HET) and *Phr1*^{C4629A/C4629A} (HOM) mouse embryonic fibroblasts (MEFs) and neuroblastoma SH-SY5Y cells (CRISPR KO and WT) (left). An alternative in-house antibody²⁵ was also used to assess Phr1 expression levels across genotypes (right). **b**, Experimental work-flow used to generate activity-based**

1 proteomic data presented in Figure 5b. **c**, Extracted proteomes from MEF with indicated
2 genotypes were treated with a maltose-binding protein (MBP)-tagged activity-based probe.
3 MBP tagging was necessary to discern a gel shift upon MYCBP2/Phr1 (0.5 MDa) labelling.
4 ABP labelling was selectively abolished in *Phr1*^{C4629A/C4629A} MEFs consistent with the E3 ligase
5 activity being disrupted. This experiment was carried out twice with similar results. **d**,
6 NMNAT2 with a C-terminal HA-tag was transiently transfected into MEFs representing all
7 three genotypes. This experiment was carried out once. **e**, The number of secondary branches
8 (gray) between the primary branches (black) crossing the red dotted line were counted.
9 Quantification of secondary axonal branches of the right phrenic nerve; *n* number per genotype
10 are indicated in the figure (mean ±SEM; Kruskal-Wallis test followed by Dunn's multiple
11 comparison test). Asterisks indicate: * $P \leq 0.05$.
12
13
14
15